Progress toward a better understanding of the urea oxidation by electromediation of Ni(II)/Ni(III) system in alkaline media

Guillaume Hopsort, Diana Pereira Do Carmo, Laure Latapie, Karine Loubière, Karine Groenen Serrano, Theodore Tzedakis

Progress toward a better understanding of the urea oxidation by electromediation of Ni(II)/Ni(III) system in alkaline media

Guillaume Hopsort[a,*], Diana Pereira Do Carmo[a], Laure Latapie[a], Karine Loubière[a], Karine Groenen Serrano[a], Theodore Tzedakis[a,*]

Laboratoire de Génie Chimique, Université de Toulouse, CNRS, INPT, UPS, Toulouse, France

*Corresponding authors:

Pr. Theodore Tzedakis, theodore.tzedakis@univ-tlse3.fr

PhD. applicant Guillaume Hopsort, guillaume.hopsort@univ-tlse3.fr

Highlights

- Urea oxidation by nickel electromediation
- Decoupling of $Ni^{(II)}$ electro-oxidation step from heterogeneous urea oxidation step
- Cyanate, ammonium, carbonate and nitrite ions as main byproducts of urea oxidation
- Measuring the apparent kinetic constant of urea oxidation
- Determining activation energies and diffusion coefficients

Abstract

Current treatments of wastewater containing urea are energy intensive and release significant quantities of gaseous nitrous oxide. The anodic oxidation of urea by electromediation of $Ni^{(III)}/Ni^{(II)}$ system in alkaline media is a promising alternative: the nitrogenous pollution is decreased while producing hydrogen at the cathode. Firstly, this study aims to deeply investigate the phenomena occurring at the interface, between electrode and electrolyte, in particular by proposing an original methodology enabling to separately study both steps, *i.e.*, the $Ni^{(II)}$ electro-oxidation and the subsequent indirect heterogeneous urea oxidation. Indeed, the variation the potential scan rate, enables *(i)* to study the effect of the operating parameters (concentration, temperature, angular velocity of a rotating disk electrode) on the rate of each mechanism step, and to *(ii)* determine key parameters of the overall process (activation energy, diffusion coefficient,

anodic charge transfer coefficient and heterogeneous electron transfer rate constant). In a second time, results of urea electrolysis exhibiting high (~80%) urea conversions, carried out at laboratory scale (1.4 g of urea) are discussed. The effect of some operating parameters (alkalinity, temperature, presence of an anionic separator or not) is examined, thanks to a set of analytical methods developed to establish complete mass balances of the products on the liquid phase. Cyanate, ammonium, carbonate and nitrite ions are identified to represent more than 80 % of the destroyed urea. Their respective quantities appear to be dependent of the operating conditions. This study constitutes an essential preliminary step before designing urea electrochemical process operating at larger scale.

Keywords

Urea electro-oxidation

Mediation of Ni(II)/Ni(III)

Decoupling mechanism steps

Kinetic parameters

Degradation byproducts

Graphical abstract

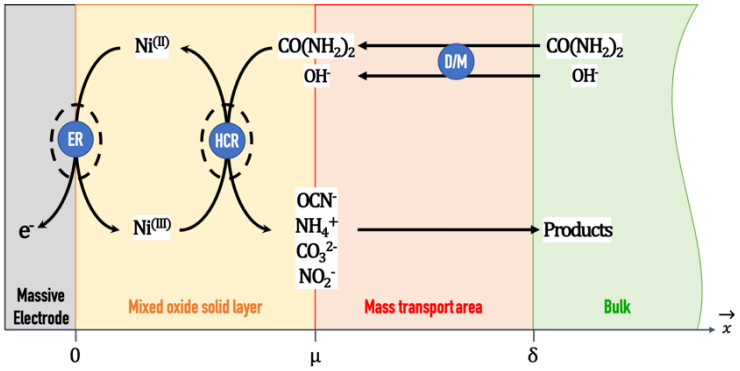

1. Introduction

The world population has been growing for many years, from 2.6 billion people in 1950 to 7 billion in 2011 and should end up, according to United Nations estimates, at 11 billion people in 2100 [1]. This population growth, which is a consequence of medical progress and improved living standards, underlines the importance of a better management of the Earth's natural resources. The associated (over)consumption of energy inevitably leads to recycling issues that should be addressed to ensure a peaceful future for next generations.

In particular, innovative solutions have to be found to transform waste into valuable products, thus limiting man's carbon footprint. Among these wastes, wastewater is today recognized as a vast field of possible revalorization. Nearly 75% of the nitrogen present in wastewater come from human urine, resulting from the filtration of blood at the kidneys [2]. This fluid is characterized by a complex composition, where more than 70 molecules have been identified such as organic compounds (urea 36.2 *wt*%, creatinine 4.1 *wt*%, creatine 1.0 *wt*%), inorganic salts (NaCl 21.5 *wt*%, K_2SO_4 7.1 *wt*%, KCl 4.4 *wt*%), and organic ammonium salts (ammonium hippurate 3.3 *wt*%, ammonium citrate 2.0 *wt*%, ammonium glucuronate 1.7 *wt*%) [3], and presents a great variability for the same individual (diet, time of collection, etc.) and between each individual (age, diet, sex, etc.) [4]. Multiple methods of urea degradation have emerged to face with the related large amount of nitrogen pollution produced every day. One can cite hydrolysis [5], enzymatic decomposition [6], biological treatment, chemical oxidation [7], adsorption [8,9], catalytic decomposition [10]. However, these processes require either expensive equipment and/or high energy consumption, or are not mature for industrial scale-up.

In this context, electrochemical oxidation is a promising alternative for pollution removal in wastewater, as it offers the advantage of a relatively simple implementation at room temperature, thus boosting the attention of the electrochemical community over the last decade [11–14]. In general, the anodic half-electronic reaction enables pollutants degradation (industrial, human, or animal waste) while the cathodic half-electronic reaction enables producing hydrogen, that can be used later as fuel.

A key practical requirement for the urea electro-oxidation (UEO) is the availability of highly efficient and cost-effective electrocatalysts. From an environmental perspective, neutral media would be preferred for UEO, as it does not involve corrosive and environmentally toxic electrolytes. In this case, platinum [15] or boron-doped diamond [16] are generally used. However, these materials are expensive, making the development of this method at larger scale uneconomic. By performing the urea electro-oxidation in alkaline environment, the use of precious metals for the electrodes is not mandatory [17,18], which drastically reduces the economic cost of the process and opens many prospects for transposition to an industrial scale. Nickel-based alloys have the advantage of being cheap, widely available and offer the ability to remove the critical urea waste while producing hydrogen at a lower cell voltage than that required for water splitting [19]. The reaction of the UEO on Ni-based electrodes has been studied using various methodologies (in situ X-ray diffraction [20], in situ surface-enhanced Raman spectroscopy [21,22], density functional theory [23], potential oscillations [24]), from which two mechanistic pathways have been suggested, including direct and indirect urea oxidation on nickel.

Direct oxidation :

At the anode : $CO(NH_2)_2 + 6OH^- \rightarrow N_2 + 5H_2O + CO_2 + 6e^-$ (1)

At the cathode: $6H_2O + 6e^- \leftrightarrow 3H_2 + 6OH^-$ (2)

Overall: $CO(NH_2)_2 + 6e^- \rightarrow N_2 + 3H_2 + CO_2$ (3)

Indirect oxidation

At the anode: $(Ni(OH)_2 + OH^- \leftrightarrow NiOOH + H_2O + e^-) \times 6$ (4)

$6NiOOH + CO(NH_2)_2 + H_2O \rightarrow 6Ni(OH)_2 + N_2 + CO_2$ (5)

Anodic overall: $CO(NH_2)_2 + 6OH^- \rightarrow N_2 + 5H_2O + CO_2 + 6e^-$ (6)

At the cathode, the reaction, represented in Eq. (2), occurs and the overall reaction is the same as Eq. (3). The indirect route is the most studied, in particular to highlights the catalytic behavior of the nickel oxyhydroxide (NiOOH) intermediate [23,25–27].

Recently, studies have been carried out for designing Ni-based catalyst with enhanced performances, following two main strategies *(i)* increasing the specific electroactive surface of the electrodes and thus the

current density by using porous and nanostructured structures [28–31] and *(ii)* to design anode materials, especially electrodeposited alloys such as Ni-Co [32], Ni-Zn [33], Ni-Carbon sponge [34] or Ni-W [35], enabling to reduce the anodic overvoltage of the urea electro-oxidation, so as to make future processes economically viable.

As highlighted in the review of Urbańczyk [36], most of the papers published on UEO report investigations at laboratory scale. Interestingly, the occurrence of byproducts is analyzed in neutral and acidic electrolytes (such as CO_2, N_2, H_2, OCN^-, NO_3^-, NO_2^-, $N_2O_2^-$, N_2O or NO_2). However, few works [36–38] have characterized byproducts in alkaline medium (such as OCN^-, NH_4^+, NO_2^- and CO_3^{2-}). The validity of the results related results appears relatively limited, mainly because *(i)* the achieved urea conversion in these works remains low (< 10%) and *(ii)* no complete mass balance has been performed.

In this context, this paper aims at investigating the treatment of urea by electro-oxidation on $Ni^{(II)}/Ni^{(III)}$ system in alkaline medium. The main objective is to get a better understanding of the electro/chemical mechanisms and kinetics of the oxidation of the urea by the electromediation of the system $Ni(OH)_2$/NiOOH. For that, this work is going *(i)* to introduce the turn over number and determine the activation energies (chemical reaction and material transport). In addition, the electrochemical characteristics of the NiOOH/$Ni(OH)_2$ system (heterogeneous electron transfer rate constant and anodic charge transfer coefficient), which is not done in the existing literature ; *(ii)* to carry out lab-scale electrolysis exhibiting high (>80%) urea conversion on massive nickel electrode, and consequently *(iii)* to open new analytical roads to detect the whole electrogenerated products in liquid phase and to perform the corresponding mass balances.

By this way, it is expected to validate the process at the lab-scale (70 cm^3 of urine) which constitutes a preliminary step before designing a urea electrochemical process operating at larger scale, namely able to treat 5 L of urine.$days^{-1}$.$m^{-2}_{electrode}$. For this purpose, three experimental set-ups are implemented either for the electrochemical kinetic study and lab-scale electrolysis using both undivided and divided electrochemical cell. A set of analytical techniques (ionic chromatography and total organic carbon) is

developed in order to identify the products electrogenerated, determine their concentration and the urea conversion.

Firstly, a characterization of the studied electrochemical system is presented through voltammetry experiments; the influence of the potential scan rate, the concentration of reactants and rotational speed is particularly studied. Secondly, lab-scale electrolysis, for which complete mass balances are systematically established, are performed. In these experiments, a special attention is paid for varying the concentrations of urea and KOH in a large range, as well as the temperature and of the presence of a membrane separator.

2. Experimental

In Appendix A, details concerning chemicals (of Normapur® grade) are reported (Table A.1), as well as the physicochemical properties of aqueous solutions of urea in alkaline medium (Figs. A. 1-3).

2.1. Experimental set-ups

All the electrochemical experiments were performed using a PGSTAT 128 N potentiostat (Metrohm Autolab®) controlled by NOVA software. A reference electrode Hg/HgO (Origasens, Origalys®) located inside a Luggin capillary containing support electrolyte (1 mol.L^{-1} of KOH), and all the potentials were given with respect to Hg/HgO ($E^{\circ}_{Hg/HgO}$ = 107 mV *vs SCE* for NaOH 1 mol.L^{-1} [39]). Three configurations of electrochemical cell were used, as schematically presented in Fig. 1. Pictures of these setups are also available in Appendix B (Fig. B.1).

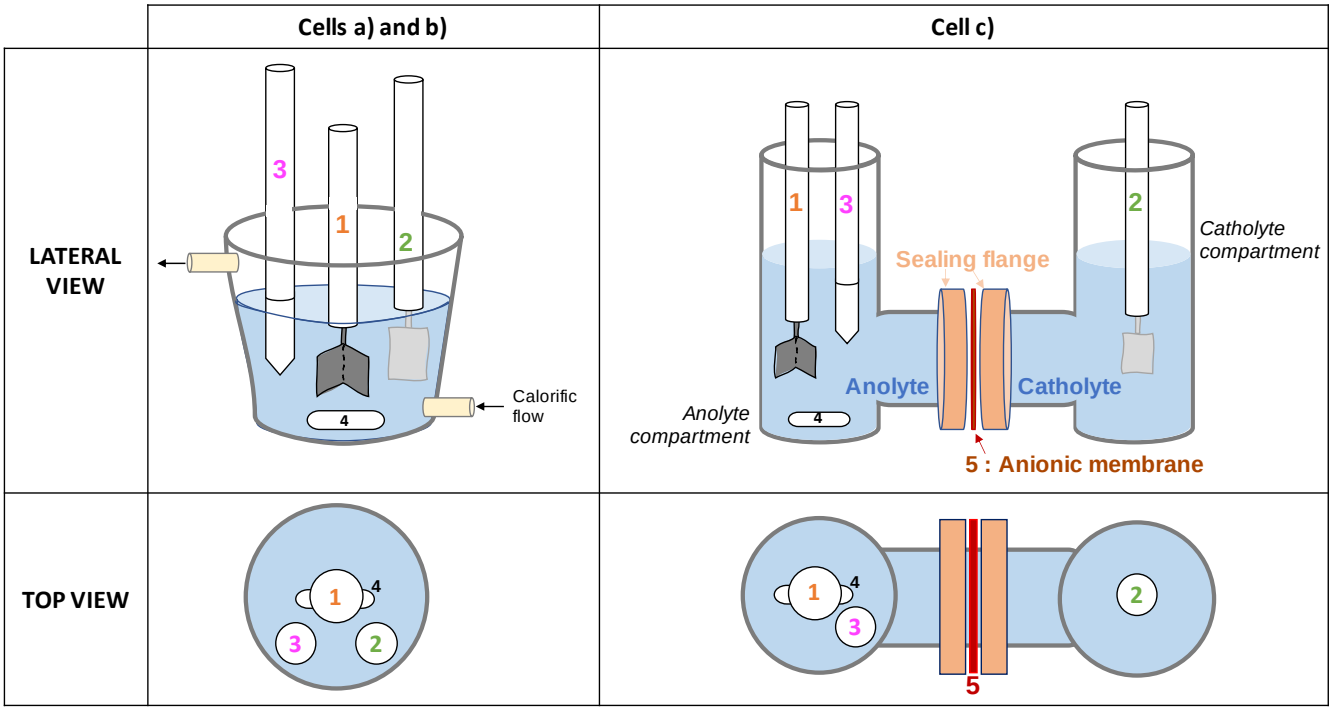

Fig. 1. Experimental setup used for a) i-E curves b) undivided cell for preparative electrolysis c) un/divided cell for preparative electrolysis. Working electrode (WE) and counter electrode (CE) are identified as 1 and 2. Reference electrode is labelled 3. In the case of electrolysis, a magnetically stirring bar (mark 4) was used to mix the electrolyte solution. In case of divided cell, the membrane separator (mark 5) holds in place by flanges that maintain the seal.

Cells a) and b) were conventional three-electrodes thermoregulated cells (Metrohm type cell). All the voltammograms were repeated 3 times. The temperature of the solution was regulated by the circulation of a thermostatic solution in the double-jacketed electrochemical cell.

Cell a) was used for voltammetry, the electrolyte volume was 50 mL. The working electrode (WE) was a rotating Ni disk (2 mm diameter) sealed in a Teflon rod, while the counter electrode (CE) consisted of a Pt rod (40 mm^2).

Cell b) was implemented for carrying out preparative electrolysis at the lab scale (around 1.4 g of urea). To that end, two massive nickel plate (4 and 15.7 cm^2) were used as anode in this study. Both anode and cathode (Pt 2 cm^2) were introduced into the cell without any separator. A magnetically stirring bar was placed at the bottom of the cell, allowing a controlled agitation at 500 RPM.

Cell c) was a H-shaped cell with the same electrodes than cell b) and with a membrane separator module placed between anolyte and catholyte compartments. Such design was used for the comparison between undivided or divided cell configurations in terms of urea degradation. The anionic nature of the membrane

(IONAC MA-375, Lanxess®) allowed migrating OH^- ions produced at the cathode and consumed at the anode, while separating the other species. The anolyte was stirred using a magnetically stirring bar at 500 RPM. Note that, for rightly comparing both configurations, a special care was required to operate with constant volume in both divided ($V_{anolyte}$ = 70 mL) and undivided ($V_{electrolyte}$ = 70 mL) cells, while conserving unchanged the electroactive surface.

Electrolytes were alkaline solutions of KOH prepared at concentrations in range of 0.5 to 5 $mol.L^{-1}$. Solutions including urea were prepared at the concentration close to those into the human urine. (*i.e.*, 0.33 $mol.L^{-1}$ [40]).

2.2. Analytical methods

A set of analytical methods were defined and optimized in order to quantify the electrogenerated products and to carry out complete mass balances. Two of the used methods were detailed below.

2.2.1. Ionic chromatography

The electrogenerated ionic intermediates were identified and quantified using a ThermoScientific® ICS 5000 with a conductimetric detector.

For cation analysis, the mobile phase used was a 30 $mmol.L^{-1}$ methanesulfonic acid solution flowing in isocratic mode (1 $mL.min^{-1}$ at 313 K) across a CS16 column (5×250 mm). The anion column was an AS19 (2×250 mm) and the flow rate was 0.25 $mL.min^{-1}$ at 298 K. The mobile phase was produced by a potassium hydroxide generator, composed of a high-pressure KOH generation chamber and a low-pressure K^+ electrolyte reservoir. The generation chamber and the electrolyte tank contained respectively a cathode where hydroxide ions were generated following reaction in Eq. (7), and an anode in a K^+ electrolyte solution.

$$2H_2O + 2e^- \rightarrow H_2 + 2OH^- \quad (7)$$

To generate a KOH eluent, deionized water was pumped through the KOH generation chamber and a direct current was applied between the anode and cathode of the eluent cartridge. A cation exchange membrane

allowed the K^+ ionic transfer to the catholyte, and the formed KOH was transferred to the high-pressure generation chamber. At the anode, the water oxidation released oxygen gas.

A concentration gradient of the eluent flowing across the column was applied (see Table 1) to optimize the elution of compounds with close column's affinity.

Table 1 Applied gradient of the KOH concentration for anionic analysis

Duration (min)	0 → 2	2 → 10	10 → 13	13 → 15	15 → 17	17 → 18
[KOH] (mmol.L^{-1})	15	15 → 20	20 → 50	50	50 → 15	15

The overall duration of the analysis was 18 min. Typical temporal profiles of the eluent concentration, as well as cation chromatogram, anion chromatogram and calibration curves are illustrated in Appendix C. (Fig. C. 1-2)

2.2.2. Non Purgeable Organic Carbon

The carbon present in aqueous solution could be identified in form of total organic carbon (TOC) and inorganic carbon (IC). Organic carbon had bonds with hydrogen and oxygen to form organic molecules (proteins, lipids, carbohydrate molecules, nucleic acids) while inorganic carbon was encountered in the form of dissolved carbon dioxide, carbonic acid, bicarbonate and carbonate. The measurement of TOC, considered as an indicator of mineralization of the solution, could be refined by distinguishing *(i)* purgeable organic carbon (referring to the organic carbon that was sparged or removed from a sample, such as volatile acids or solvents) from *(ii)* non-purgeable organic carbon (noted NPOC, and referring to the organic carbon remaining in an acidified sample after purging the sample with carbon-free gas).

The mineralization of carbon contained in urea could be then monitored by the variation of NPOC following protocol consisted of two steps: *(i)* an alkaline sample (high carbonate concentration through carbonation) was acidified by adding hydrochloric acid in order to obtain a pH lower than 3 and *(ii)* synthetic air except of CO_2, was bubbling through the sample during 7 min to convert POC and IC into gaseous dioxide carbon according to Eq. (8) followed by Eq. (9).

$$CO_3^{2-} + 2H^+ \leftrightarrow CO_{2,dissolved} + H_2O \quad (8)$$

$$N_2 + O_2 + CO_{2,dissolved} \leftrightarrow N_2 + O_2 + CO_{2,gas} \quad (9)$$

Measurements were performed using a SHIMADZU® TOC-L. Carrier gas flowed at 150 mL.min^{-1} inside the combustion tube, filled with an oxidation catalyst (alumina beads with 0.5% of Pt) and heated to 953 K. The sample was then burn in the combustion tube to form carbon dioxide. Combustion products, contained in the carrier gas, flowed from the combustion tube to the dehumidifier. The whole gas passed through a halogen scrubber before reaching the cell of non-dispersive infrared (NDIR) gas analyzer, where the dioxide carbon was detected. The analog signal of the NDIR formed a peak which area was proportional to the NPOC concentration. Hence, after establishing a calibration curve with different urea solutions at pH 14, the NPOC related to a given sample could be measured directly from the peak area.

It was verified, and shown in Appendix D, that the NPOC measurement represented only the urea concentration, and that the presence of reaction intermediates (at different concentrations) did not affect this measurement (Table D.1).

3. Results and Discussion

3.1. Effect of the operating parameters on the voltammogram shapes

In this section, the involved electrochemical system is characterized through voltammetry experiments. The influence of the scan rate, the concentration of reactants, temperature and agitation speed on the overall rate of the urea indirect electro-oxidation is studied, expecting to elucidate the mechanism of the process.

3.1.1. Effect of urea concentration on overall rate of the indirect electro-oxidation

The effect of the urea concentration on the rate of the overal process is examined by plotting voltammograms on nickel RDE, in 1 mol.L^{-1} KOH solutions at a scan rate of 1.36 mV.s^{-1}. Fig. 2 shows the obtained voltammograms for urea concentrations ranging from 0 to 0.33 mol.L^{-1}.

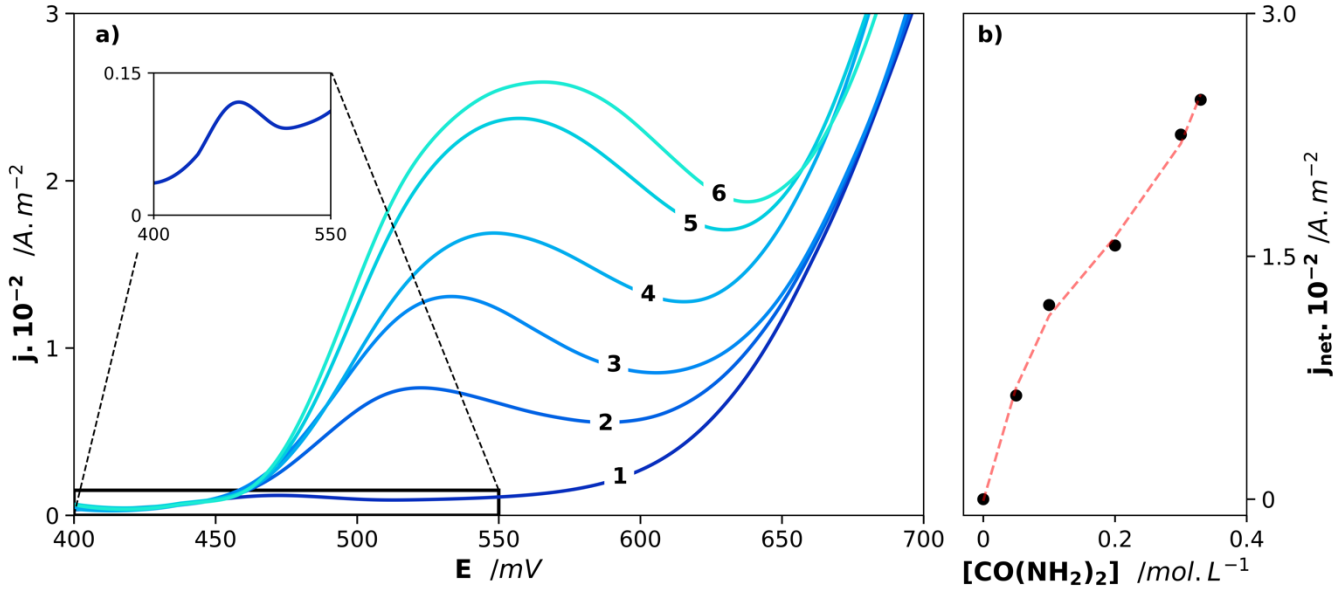

Fig. 2. Effect of the urea concentration a) on the shape of voltammograms obtained on nickel RDE without agitation. [KOH] = 1 mol.L^{-1}; v = 1.36 mV.s^{-1}; T = 298 °K, S = 3.14 mm^2. The urea concentration used was 0 mol.L^{-1} (1), 0.05 mol.L^{-1} (2), 0.1 mol.L^{-1} (3), 0.2 mol.L^{-1} (4), 0.3 mol.L^{-1} (5) and 0.33 mol.L^{-1} (6). Fig. 2-b) shows the evolution of the intensity of the oxidation peak as a function of the urea concentration.

Curve **1** (without urea), obtained on a nickel RDE freshly polished, exhibits a signal showing a peak at ~ 470 mV. According to Seghiouer et al. [41], this peak corresponds to the oxidation of $Ni^{(II)}$ to $Ni^{(III)}$ following the reaction Eq. (4). The oxidation of $Ni^{(0)}$ into $Ni^{(II)}$, Eq. (10), occurs theoretically at potentials close to - 800 mV.

$$Ni + 2\,OH^- \rightarrow Ni(OH)_2 + 2\,e^- \qquad (10)$$

Note that this signal peak at ~ 475 mV is attributed [42] to the reaction Eq. (4). For higher potentials (> 600 mV), the solvent oxidation to oxygen occurs.

If the nickel oxidation signal is observed at such high potentials (400 mV), this means that, immediately after polishing, the nickel surface is spontaneously oxidized by the oxygen of the air, and that the nickel is covered by some oxides. Consequently, the observation can be translated by the reaction Eq. (11).

$$Ni_xO_y + (2x - y)OH^- \rightarrow xNiOOH + (2x - y)e^- \qquad (11)$$

Curves **2** to **6**, obtained when urea was added at various concentrations into the the electrolyte, exhibit peaks shifting to the anodic potentials as the urea concentration increases, while the solvant oxidation potential

does not seem to be affected. Note that the KOH concentration (1 mol.L^{-1}) is three times more concentrated than the highest concentration of urea used (0.33 mol.L^{-1}).

The variation of this peak current (from which the blank have been substracted) *vs.* the urea concentration, plotted in the Fig. 2-b, does not show a linear behavior, meaning that the observed signal may not be attributed to a single direct oxidation of urea as already demonstrated [43] for urea concentration higher than 0.33 mol.L^{-1}. Consequently, a catalytic process occurs at the electrode: urea is oxidized chemically by the nickel peroxide at the electrode surface and gives products while regenerating $Ni(OH)_2$.

In order to get a better understanding of the overall process, the oxidation of urea by the electromediation of the system $Ni(OH)_2$/NiOOH in alkaline medium consisted of an indirect or two-step mechanism, could be schematically [44] represented, according to Fig. 3.

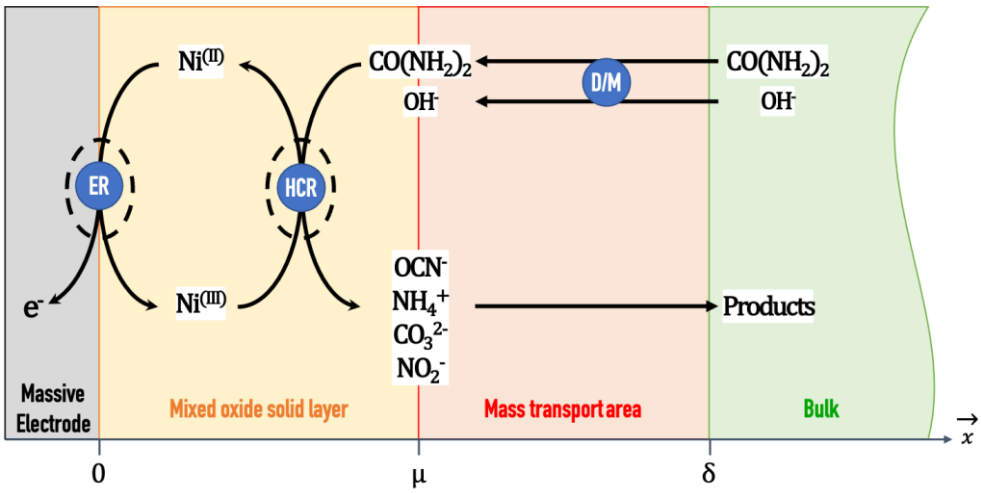

Fig. 3. Schematic representation of the indirect oxidation of the urea, by the electromediation of the system $Ni(OH)_2$/NiOOH operating on the surface of a massive nickel anode, and in presence of alkaline medium. ER, HCR, and D/M indicate respectively the locations where the NiOOH electrogeneration reaction, the heterogeneous catalytic reaction and the mass transport (limited by the diffusion) take place.

Various phenomena occur during the UEO on a massive nickel anode and their locations depend to the distance from the massive electrode (*i.e.*, *x*-axis dependent):

- at $x = 0$, the massive Ni surface is oxidized to successively form $Ni(OH)_2$ and NiOOH;
- $0 < x < \mu$ corresponds to the thickness of the catalytic system $Ni(OH)_2$/NiOOH (solid layer), in which the chemical reaction is assumed to occur;

- $\mu < x < \delta$ corresponds to the layer in which external mass transfer limitations exist for urea (and eventually KOH); [45]
- $x > \delta$ corresponds to the bulk (none reaction occurs).

After the 'first spontaneous' oxidation of metallic Ni and the electrogeneration of NiOOH, three phenomena are expected to occur: an electrochemical reaction (ER) involving insoluble oxides (Eq. (12)), heterogeneous chemical reactions (HCR) occurring into the solid layer of NiOOH (Eq. (13)), and as function of the operating conditions, a mass transfer process (D/M) (Eq. (14)).

ER: $$Ni(OH)_2 + OH^- \rightarrow NiOOH + e^- + H_2O \quad (12)$$

HCR: $$CO(NH_2)_2 + 8OH^- + 6NiOOH \rightarrow 6Ni(OH)_2 + N_2 + CO_3^{2-} + 6H_2O + 6e^- \quad (13)$$

D/M: $$\begin{cases} \frac{\partial[\mathrm{CO(NH_2)_2}]}{\partial \mathrm{t}} + \nabla . \mathrm{j_{D,CO(NH_2)_2}} = 0 \\ \frac{\partial[\mathrm{OH^-}]}{\partial \mathrm{t}} + \nabla . (\mathrm{j_{M,OH^-}} + \mathrm{j_{D,OH^-}}) = 0 \end{cases} \quad (14)$$

Where j_i is the molar flux (diffusion or migration) of the species i (mol.m^{-2}.s^{-1}).

Each elementary process being dependent of the other, it is therefore important to understand how a given operating parameter could impact each of them. In alkaline medium, note that the reaction Eq. (13) represents the global equation, namely the one corresponding to a complete mineralization of urea involving 6 electrons and produce carbonates (6 OH^- involved in Eq. (6) *vs* 8 OH^- involved in Eq. (13)).

3.1.2. Highlighting the catalytic system: scan rate as a tool for revealing the limitation of the HCR on the ER

To confirm previous assumptions and validate the overall process schema reported Fig. 3, the effect of the scan rate, *v*, is examined in the cases of the blank (NiOOH/KOH, Fig. 4-a) and an alkaline solution of urea (NiOOH/KOH/Urea, Fig. 4-b).

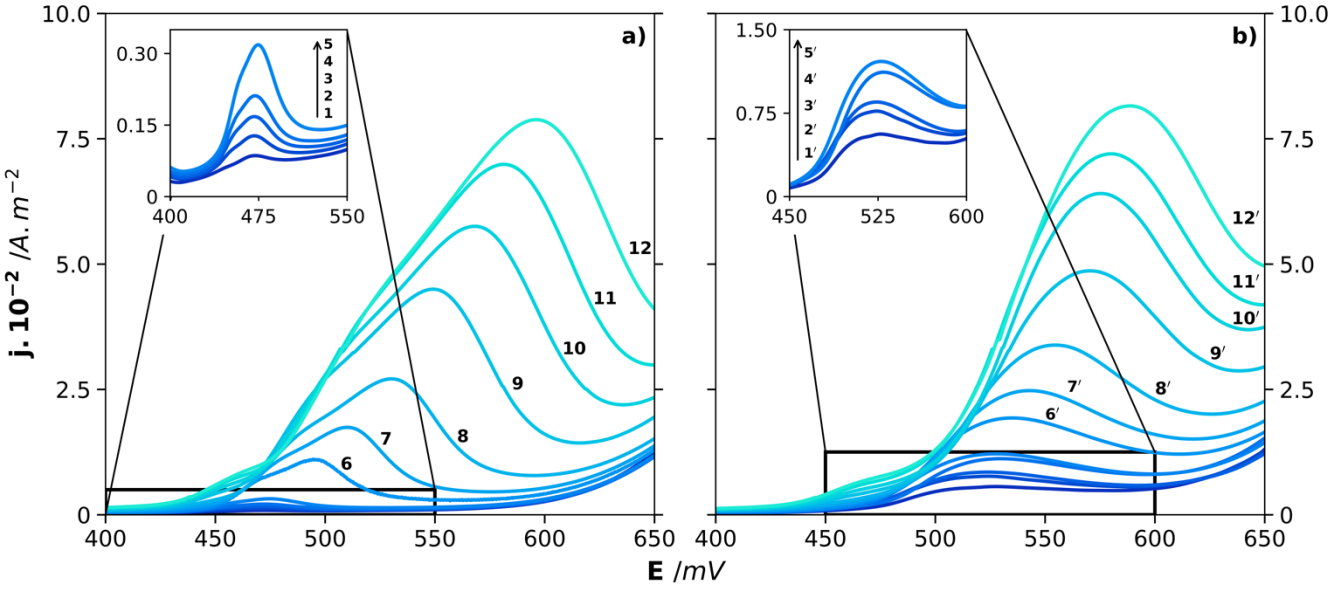

Fig. 4. Effect of potential scan rate on the voltammograms obtained without agitation on nickel electrode immersed into a) in 1 mol.L^{-1} KOH solution b) in 1 mol.L^{-1} KOH containing 0.05 mol.L^{-1} of urea. The scan rate used was 0.58 mV.s^{-1} (1-1'), 1.36 mV.s^{-1} (2-2'), 2.16 mV.s^{-1} (3-3'), 2.91 mV.s^{-1} (4-4'), 5 mV.s^{-1} (5-5'), 25 mV.s^{-1} (6-6'), 50 mV.s^{-1} (7-7'), 100 mV.s^{-1} (8-8'), 200 mV.s^{-1} (9-9'), 300 mV.s^{-1} (10-10'), 400 mV.s^{-1} (11-11') and 500 mV.s^{-1} (12-12'). The insets show a zoom in the oxidation peaks at low potential scan rate.

Regarding the voltammogram obtained in a KOH solution without urea (Fig. 4-a), a complex signal is observed containing two shoulders and one peak respectively, at about 460 mV, 475 to 525 mV and, 480 to 600 mV depending on ν. The initial surface of the Ni, even polished, appears to be partially oxidized and the oxidation of the various intermediates (Eq. (11)) could be responsible of the observed shoulders. Whatever the oxidation state of the surface, the final product is $Ni^{(III)}$. Moreover, the main peak is attributed to the oxidation of the $Ni^{(II)}$ to $Ni^{(III)}$.

Conversely, resolute peaks are observed on the curves obtained with urea (Fig. 4-b) . It seems that, as reacting with nickel peroxide and thus regenerating the reagent $Ni(OH)_2$, urea allows to obtain only one predominant redox system.

As showed by the reaction Eq. (12), $Ni(OH)_2$ oxidation requires a hydroxide ion. As a result, the quasi-cancellation of the current density for potentials ranging from 600 to 650 mV depending on the scan rate, could also be caused by the complete coverage of the anode surface by NiOOH, as already mentioned in various works [46,47]. Note that in both cases (Fig. 4-a and b) at the end of the signal, the current decreases, meaning that mass transfer limitation exists. As the electrode reaction requires hydroxide ions, one could

assume that the OH^- diffusion causes the current decrease. Besides, both the current and the potential of the peaks (Fig. 4-a and b) increase as the potential scan rate increases.

Regarding the evolution of peak potentials as function of $log(v)$, illustrated in the Fig.E.1 (see Appendix E), in the case of the NiOOH/urea system, extracted from Fig. 4-b, a linear evolution (Eq. (15), R^2 = 0.995) was observed between the potential of the anodic peak and the logarithm of the potential scan rate.

$$E_{peak} = 0.04 \times \log(v) + 0.60 \qquad (15)$$

The variation of the potential against the potential scan rate is relatively low and the obtained slope (0.04) is ten times lower than the theoretical value (0.5), meaning that the corresponding $Ni(OH)_2$/NiOOH system is slightly irreversible.

The evolution of the current magnitude of the peak as a function of the potential scan rate, shown in Fig. F.1 (see Appendix F) is linear for scan rates higher than 100 $mV.s^{-1}$ with a mean slope of 4.10^{-3}. This behavior could characterize an electrochemical reaction of *(i)* adsorbed species on the anode surface or *(ii)* a thin layer of an electroactive species. Here, the system NiOOH/$Ni(OH)_2$ is considered to be two adsorbed species at the nickel surface. Consequently, this demonstrates that at high scan rates the electrochemical reaction ($Ni(OH)_2$→NiOOH) is the limiting step of the overall process of the urea indirect electrooxidation.

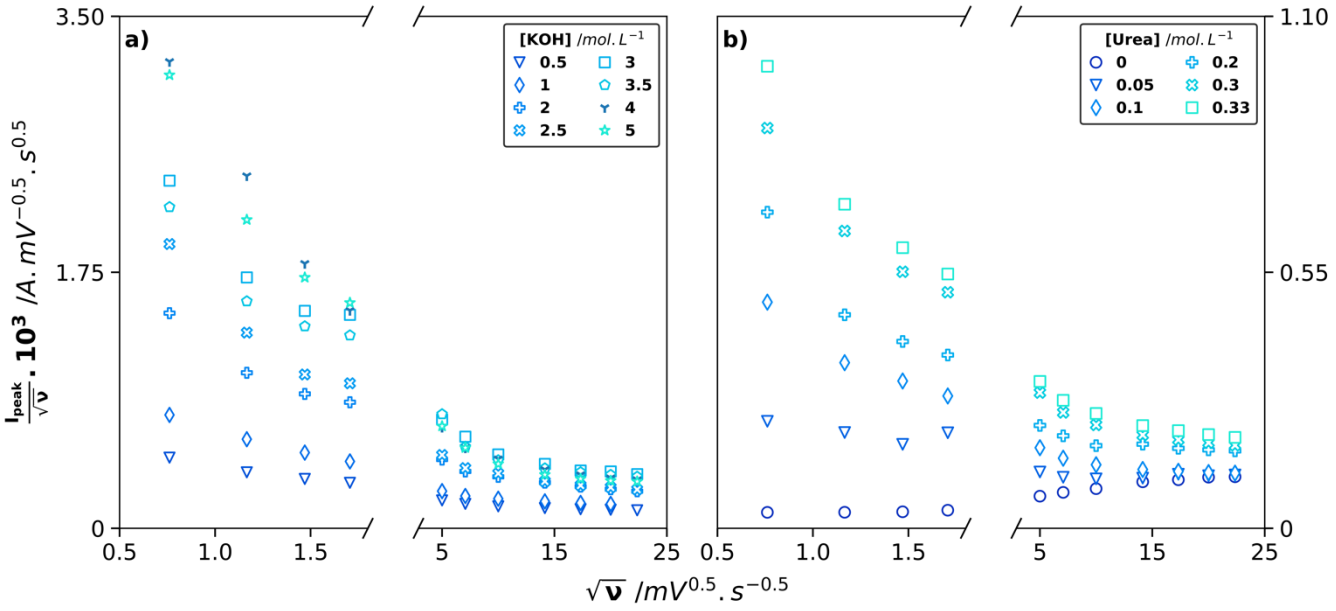

Fig. 5. Evolutions of the ratio between the current magnitude of anodic peak and $\sqrt{v}$ at different concentrations of a) KOH in a solution of 0.33 mol.L^{-1} urea and b) urea in a solution of 1 mol.L^{-1} KOH . Results extracted from the current potential curves (not shown here) were plotted for various concentrations of a) KOH from 0.5 to 3 mol.L^{-1} or b) urea from 0 to 0.33 mol.L^{-1}.

The effect of the potential scan rate is also studied for various KOH concentrations as well as urea, in order to get a better highlight of the overall process, *i.e.*, the HCR ($Ni^{(III)}$/Urea) coupled to the ER ($Ni^{(III)}/Ni^{(II)}$). The influence of v on the peak current is plotted in Fig. 5, for the various concentrations of reagents (voltammograms are not illustrated here). For a 'simple' electrochemical reaction, the normalized peak current by the square root of the potential scan rate, $\frac{I_p}{\sqrt{v}}$, is expected to be constant against the square root of the potential scan rate, $\sqrt{v}$ [48,49]. In the present case, the results do not present a linear variation in the whole examined range of v. For potential scan rates in the range of 100 to 500 $mV.s^{-1}$, the experimental variation of $\frac{I_p}{\sqrt{v}}$ against $\sqrt{v}$, can be considered as linear in agreement with the theory. This means that for high v, the dominant process is the electrochemical oxidation of the $Ni^{(II)}$ to the $Ni^{(III)}$. Decreasing v seems to complexify the overall process, as, at scan rates lower than 25 $mV.s^{-1}$, the values of $\frac{I_p}{\sqrt{v}}$ decreases with $\sqrt{v}$ and this phenomenon is more pronounced at higher concentrations of both KOH (Fig. 5-a) and urea (Fig. 5-b).

This behavior is characteristic of a heterogeneous electron transfer followed by a chemical reaction which regenerate the reagent, thus increasing the current. Based on the work of Nicholson et Shain [50], the decrease of $\frac{I_p}{\sqrt{v}}$ *vs.* $\sqrt{v}$ is used as a diagnostic criterion to identify the mechanism of the reaction as an EC catalyzed mechanism, the catalytic chemical reaction interposed between successive charge transfer following Eq. (16).

$$\begin{cases} O + ne^- \rightarrow R \\ R + Z \rightarrow O \end{cases} \qquad (16)$$

Ohsaka et al. [51] has observed similar behavior in the study of the mechanism for the reaction of the initial stages of the electropolymerization of 1-pyrenamine.

Concerning the case of urea (Fig. 5-b), the system appears 'simpler'. Decreasing the potential scan rate enables the HCR to occur and consequently to regenerate the $Ni(OH)_2$ for starting a new catalytic cycle, following the scheme Eq. (17). Note that in the absence of urea (*i.e.*, Fig. 5-b circles label), the slight increase of $\frac{I_p}{\sqrt{v}}$ with $\sqrt{v}$ could be attributed to a capacitive behavior of the $Ni(OH)_2$/NiOOH system.

$$\mathrm{Ni^{(III)} + Substrat \rightarrow Ni^{(II)} + Products} \quad (\Delta V) \qquad (17)$$

An important parameter to characterize the $Ni^{(II)}/Ni^{(III)}$ system in the presence of urea is the turnover number (*TON*) presented in Eq. (18).

$$TON = \frac{Q_{total}}{Q_{blank}} \qquad (18)$$

It is defined as the ratio of the amount of charge Q_{total} corresponding to the whole anodic signal at 450 – 650 mV (Fig. 4-b) attributed to the oxidation of the $Ni^{(II)}$ to $Ni^{(III)}$ in presence of urea and the amount of charge Q_{blank} corresponding to the whole signal of the oxidation of the nickel without urea (Fig. 4-a). This definition implies to verify one of the two following conditions: *(i)* only one layer of the nickel oxidizes at the surface of the metal; *(ii)* if more than one layer reacts, the total volume of the reactive area ($0 < x < \mu$, Fig. 3) is entirely permeable to the dissolved reagents, without any internal mass transfer limitation.

The *TON* is thus plotted against *v* in Fig. 6.

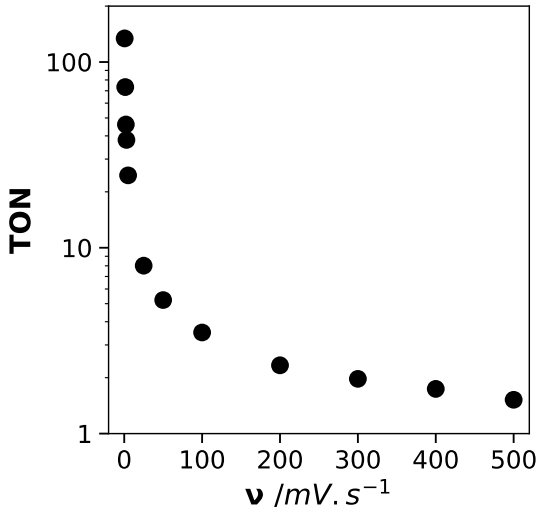

Fig. 6. Effect of the scan rate against values of TON.

Fig. 6 highlights two zones: for *v* lower than 100 $mV.s^{-1}$, high values (> 100) of *TON* are observed, while the ratio appears to tend towards 1 for *v* higher than 500 $mV.s^{-1}$. In this latter case, the electrogenerated $Ni^{(III)}$ do not have enough time to react with urea and, as the whole metallic surface is covered with $Ni^{(III)}$, the current

decreases and the *TON* tends to the unity. As the potential scan rate decreases, there is enough time for the HCR to occur (whatever the applied potentials). $Ni^{(III)}$ is reduced by urea and the electrogenerated $Ni^{(II)}$ can be oxidized again, thus enhancing the current.

Note that because: *(i)* the continuous change of the applied potential during the monitoring of the i-E curve, and *(ii)* the definition of the *TON* as a "global" parameter based on the whole amount of charge of the i-E curve, it is difficult to estimate a value of the chemical rate, r_χ, of the HCR of which the reaction scheme appears also complex (see mass balances at the next sections).

3.1.3. Effect of potassium hydroxide concentration on overall rate of the indirect electro-oxidation

Hydroxide ions are involved in both $Ni(OH)_2$ oxidation (Eq. (12)) and urea indirect oxidation by NiOOH (Eq. (13)). The last reaction exhibits a stoichiometry based on 1 mole of urea for 8 moles of hydroxide ions, meaning that the alkalinity will affect the rate of the process. In order to examine the effect of KOH on the urea oxidation current, several i-E curves are plotted, using nickel RDE with KOH concentrations ranged from 0.05 to 5 $mol.L^{-1}$, and two potential scan rates (1.36 and 500 $mV.s^{-1}$). The urea concentration chosen is 0.33 $mol.L^{-1}$ and the obtained results presented in Fig. 7.

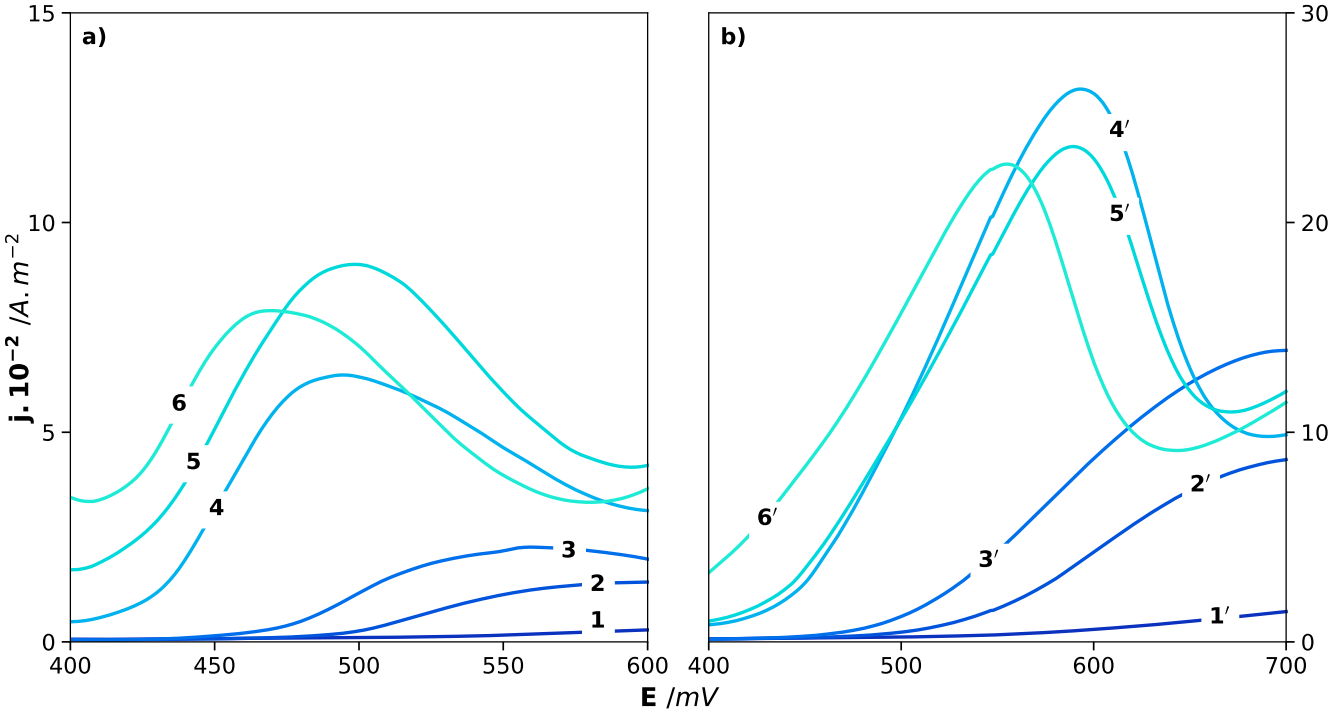

Fig. 7. Effect of KOH concentration by linear voltammogram of nickel RDE in a solution containing 0.33 mol.L^{-1} urea at a) 1.36 and b) 500 mV.s^{-1} without agitation at 298 K. The potassium hydroxide concentration used was 0.05 mol.L^{-1} (1-1'), 0.5 mol.L^{-1} (2-2'), 1 mol.L^{-1} (3-3'), 3 mol.L^{-1} (4-4'), 4 mol.L^{-1} (5-5') and 5 mol.L^{-1} (6-6').

The results show a strong effect of the KOH concentration on the shape of the curves. All the curves present, in the range from 400 to 600~700 mV, a signal meanly 'peak shaped', attributed to the $Ni(OH)_2$ oxidation to NiOOH form. Both the magnitude of the current and the potential of the peak appear to be dependent of the KOH concentration.

Indeed, for both potential scan rates, increasing the KOH concentration from 0.05 to 5 mol.L^{-1} causes a peak potential shifting to the lower potentials, meaning that the system $Ni(OH)_2$/NiOOH becomes faster.

The effect of KOH on the magnitude of the peak current of the $Ni(OH)_2$ oxidation seems more complex, two distinct area can be evidenced: the peak current increases with the KOH concentrations until reaching 4 to 5 mol.L^{-1}, and then decreases. As both reactions, in Eqs. (12)-(13), require KOH, such increase of their reaction rates with the KOH concentration is understandable, however, a 'quantitative' kinetic study would be required to deeply investigate this issue and will constitute an upcoming study.

For higher KOH concentration, the current of the curves decreases. This can be explained based on the E-pH diagram of nickel (see Fig.G.1, Appendix G) which points out that the $Ni(OH)_2$/NiOOH couple is unstable

at very high pH values. A part of this oxide can then dissolve and spread into the bulk, inducing a decrease of the rate of the anodic process.

The comparison of the voltammograms obtained at two different scan rates, ν, shows that at 500 mV.s^{-1} the signal appears as 'a more symmetrical peak' than this one obtained at 1.36 mV.s^{-1} (especially for the curves **4/4'**, **5/5'** and **6/6'**). Indeed, at 500 mV.s^{-1} and for higher potentials than 550~600 mV, the decrease of the current is due to the fact that the electrode surface (the reaction area) is completely covered/filled by NiOOH, which has not time to react with urea (the electrochemical reaction is fast, and there is no limitation by the KOH concentration). Consequently, there is no (electrogenerated) $Ni(OH)_2$ to oxidize and the current falls down, inducing the occurrence of a dissymmetric peak in the curve.

At 1.36 mV.s^{-1}, there is enough time to enable the NiOOH to react with urea and be reduced to $Ni(OH)_2$, so the current slowly decreases after 450~500 mV.

Assuming that the curves obtained at 500 mV.s^{-1} are mainly attributed to the ER (see. Eq. (12)) (i.e. without the effect of the HCR, represented Eq. (13)) and that the anodic activation limitation range of the curve obeys to the Butler-Volmer equation, the current can be expressed as Eq. (19).

$$I = n\mathcal{F}S_{reaction\ area\ for\ 0<x<\mu}k^0_{app} \times exp\left(\frac{\alpha nb}{RT}(E - E_{I=0})\right) \times \Gamma_{III} \qquad (19)$$

where: n: the exchanged electron number (dimensionless, here 1),

$\mathcal{F}$: the Faraday's constant (96 500 C.mol^{-1}),

$S_{reaction\ area\ for\ 0<x<\mu}$: the electro-active surface (m^2),

k^0_{app}: the apparent intrinsic heterogeneous electron transfer rate constant (s^{-1}), which depends on [OH$^-$] as $k^0_{app} = \frac{k^0[OH^-]^\delta}{\mu}$, where k^0 is the heterogeneous electron transfer rate constant (m.s^{-1}),

μ: the thickness (see Fig. 3) of the catalytic system $Ni(OH)_2$/NiOOH (m),

δ: the partial order of reaction Eq. (12) for hydroxide (dimensionless),

α: the anodic charge transfer coefficient (dimensionless),

E: the electrode potential (V),

$E_{I=0}$: the open circuit potential (V),

Γ_{III}: the Ni(III) surface concentration (mol.m$^{-2}_{electrode}$).

The global nickel surface concentration, Γ_0, can be expressed as Eq. (20) where Γ_{II} is the Ni(II) surface concentration.

$$\Gamma_0 = \Gamma_{II} + \Gamma_{III} \quad (20)$$

In these conditions (no chemical reaction at potential close to $E_{I=0}$ and 500 mV.s^{-1}), Γ_{III} is considered as constant and equals to Γ_0.

From Eq. (19), it comes Eq. (21).

$$\ln(I) = \left[\ln\left(n\mathcal{F}S_{reaction\ area\ for\ 0<x<\mu}\Gamma_{III}\right) + \ln(k^0_{app}) - \frac{\alpha n\mathcal{F}}{RT} \times E_{I=0}\right] + \frac{\alpha n\mathcal{F}}{RT} \times E \quad (21)$$

According to Eq. (21), the natural logarithm plot of the current (in the activation zone) *vs* potential, extracted from Fig. 7-b, is plotted Fig. 8 for [OH$^-$] ranging from 0.05 to 5 mol.L^{-1}.

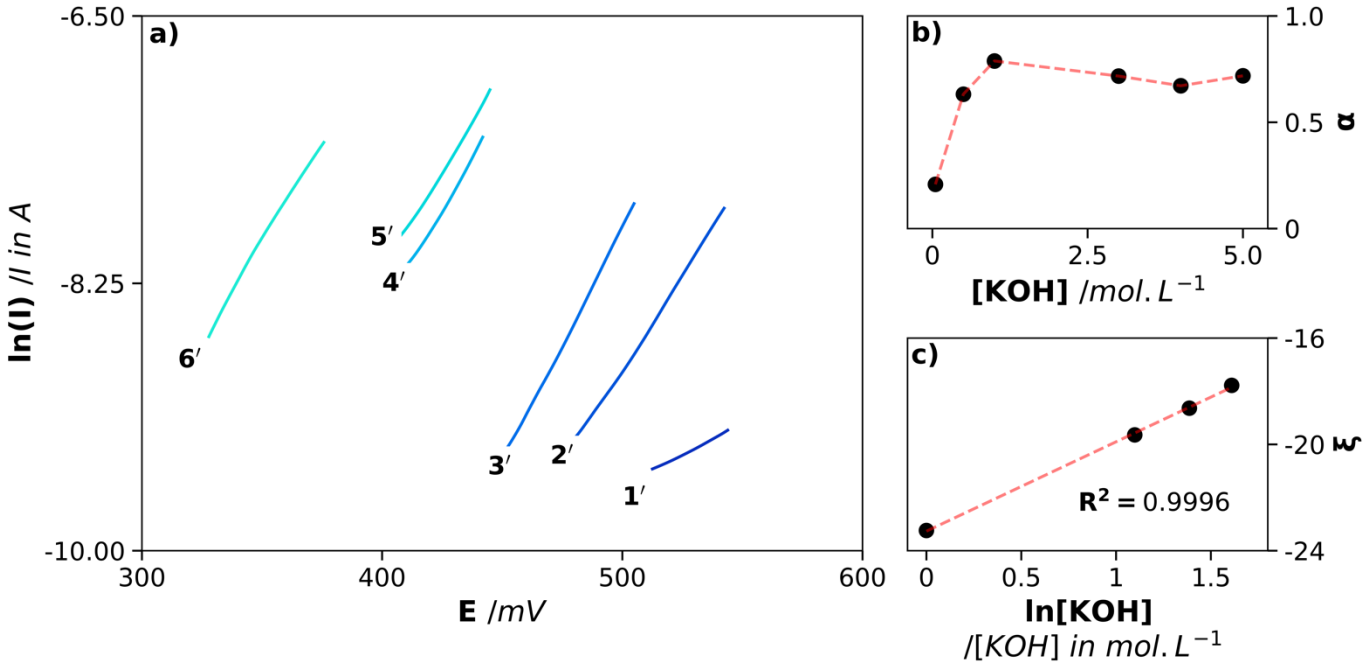

Fig. 8. a) Butler-Volmer analysis of voltammogram 1' to 6' extracted from Fig. 7-b. Figure b) shows the dependency of the anodic charge transfer coefficient α against the hydroxide concentration. Figure c) highlights the intercept of Butler-Volmer analysis against the natural logarithm of KOH concentration.

The anodic charge transfer coefficient α is deduced from the slope of the curves, as illustrated Fig. 8-a. Its variation against the KOH concentration is presented in Fig. 8-b and shows that α increases with the KOH concentration until becoming constant and equal to 0.7 at $[OH^-] \approx 1$ mol.L^{-1}. A similar value of 0.78 was obtained by Vedharathinam et al. [43]. One can note that this value is higher than 0.5 meaning a multi-step system. Other reactions can occur, such as Eq. (22), shown in the E-pH diagram of nickel [52]:

$$Ni(OH)_2 + OH^- \leftrightarrow HNiO_2^- + H_2O \quad (22)$$

The heterogeneous electron transfer rate constant k^0 and the hydroxide partial order δ in the reaction Eq. (12) are deduced from the y-intercept of the Eq. (21), noted ξ. According to Eq. (23), ξ is directly proportional to the value of the natural logarithm of the KOH concentration.

$$\xi = \left[\ln\left(\frac{S_{reaction\ area\ for\ 0<x<\mu}\Gamma_{III}k^0}{\mu}\right) - \frac{\alpha n\mathcal{F}}{RT} \times E_{I=0}\right] + \delta \times ln\,[OH^-] \quad (23)$$

The evolution of ξ against $\ln [OH^-]$ is represented in Fig. 8-c. The slope of this line, assimilated to the partial order of OH^- in the oxidation of nickel, is estimated to 3.3.

A value of 'three' would mean that three hydroxide ions are involved at the associated reaction. Taking into account the strong KOH concentrations, one can suppose that the nickel oxidized may be partially dissolved and leave the electrode surface; in this case, the bare nickel oxidizes and three electrons/OH^- would be required. This fact means that to avoid the nickel dissolution, it is preferable to carry out the urea oxidation at concentrations of KOH lower than 1 mol.L^{-1}, even if the electrochemical conditions are not the more optimum.

The value of k^0, is obtained through the y-intercept of Eq. (23), noted ξ' (i.e., $\xi' = \ln\left(\frac{n\mathcal{F}S_{reaction\ area\ for\ 0<x<\mu}\Gamma_{III}k^0}{\mu}\right) - \frac{\alpha n\mathcal{F}}{RT} \times E_{I=0}$ and estimated to -14 in this study), as Eq. (24).

$$k^0 = \frac{\mu}{n\mathcal{F}S_{reaction\ area\ for\ 0<x<\mu}\Gamma_{III}} \exp\left(\xi' + \frac{\alpha n\mathcal{F}}{RT}E_{eq}\right) \quad (24)$$

In order to estimate an order of magnitude of the reaction layer thickness, μ, the integration of i-E curves using a nickel RDE immersed in a 1 mol.L^{-1} KOH solution (Fig. 4-a), is performed and allows to obtain the

molar quantity transformed during the potential scan. Knowing the geometrical properties of the crystallographic phases from the work of Tkalych et al. [53], a thickness μ of 50 nm is obtained. $Ni(OH)_2$/NiOOH nickel metal oxides are electronic conductors. In the reaction layer of thickness μ, no electronic limitation exists [54,55].

The zero current potential is estimated from the Gibb's free energy [56] and its value is taken as 490 mV *vs SHE*. The value of k^0 is then estimated, at 298 K and with 1 e^- exchanged, to 8.1×10^{-2} $cm.s^{-1}$ a low value translating an irreversible system.

As expected, this value is much lower than 0.3 $cm.s^{-1}$ which is associated the limit of reversibility for a simple one-electron process based on the work of Dickinson et Wain [57].

3.1.4. Effect of temperature on electrocatalytic properties

The effect of temperature in the range of 298 to 313 K on the voltammograms is presented in Fig. 9-a. These curves are obtained at low potential scan rates (0.66 $mV.s^{-1}$) under stirring.

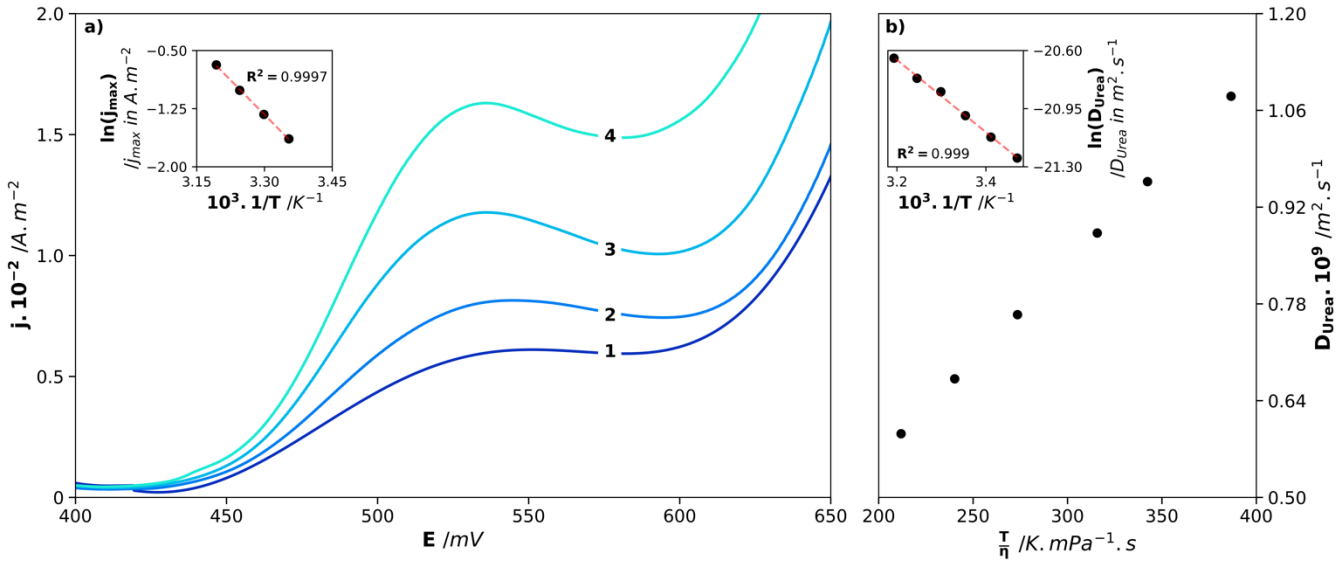

Fig. 9. a) Effect of temperature on the voltammograms obtained at 0.66 $mV.s^{-1}$, on nickel RDE in a 1 $mol.L^{-1}$ KOH solution containing 0.33 $mol.L^{-1}$ urea. The temperature used was 298 K (1), 303 K (2), 308 K (3) and 313 K (4). ω = 200 RPM. Inset: $ln(j_{max}) = f(1/T)$ plotted to determine the activation energy of the global process.
b) Temperature dependence of the urea diffusion coefficient in 1 $mol.L^{-1}$ KOH solution between 288 and 313 K obtained by viscosities measurements. Inset: $ln(D_{urea}) = f(1/T)$ plotted to determine the activation energy of the diffusion coefficient.

Note that, conversely to the previous cases (Fig. 2, Fig. 4 and Fig. 7) performed without stirring, here, the stirring enables to supply the interface with a constant flux of the dissolved reagents *i.e.*, the urea and the

hydroxide ions. Besides, the low applied potential scan rate enables to the overall catalytic cycle (Eq. (17)) to occur, thus the observed current is the overall catalytic current.

The increase in temperature leads to an increase in the overall current but does not seem to affect the position (potential) of the curves. This evolution is in agreement with the simultaneous decrease of the solution viscosity implying an increase of the diffusion flux of (electro)reactive species to the electrode. Moreover, in general, the temperature causes the increase of the chemical rate according to the Arrhenius' law.

In Curve **1** obtained at 298 K, a quasi-plateau (with a very slight decrease of the current) is observed between 520 and 570 mV, exhibiting a diffusion limited current. This means that mass transport of dissolved reagents limits the overall process. The limitation is due to the urea present in the HCR. Indeed, the ER could not be limiting because the amount of OH^- required to oxidize $Ni(OH)_2$ and regenerate NiOOH is low due to the low Γ_{II} surface concentration.

Increasing the temperature causes a deformation of the curves; typically, the current slightly decreases in the plateau area (520 and 570 mV), before reaching the oxidation potential of the solvent (600 mV), where it increases again. Note that the observed decrease of the current remains smaller than 10 % (for the highest temperature). The decrease in current can be explained by a partial passivation of the nickel anode. This phenomenon does not appear to be strong or irreversible, as the solvent oxidation occurs in the same potential range as without urea.

At least, two possibilities can be proposed to explain this partial passivation:

(i) Due to the OH^- depletion, at the limiting current, the interface may be partially neutralized and therefore carbonate, a byproduct of the HCR (see next sections) may generate a gaseous layer of carbon dioxide. In addition, a higher temperature facilitates the degassing of CO_2. The presence

of such a gaseous layer may easily reduce the diffusion flux of urea [23,58] and consequently distort the observed plateau.

(ii) The increase in temperature leads to an increase of the current and at high currents, the oxidation of urea may generate intermediates (even of small size) that would be adsorbed at the electrode and reduce the number of active nickel atoms (NiOOH), thus implying a decrease in the rate of the process.

A macroscopic mass balance of the $Ni^{(III)}$ can be expressed as Eq. (25).

$$\begin{cases} \text{Accumulation flux of } Ni^{(III)} + \text{Chemical reaction } \left(\text{consuming } Ni^{(III)}\right) \text{ flux} - \text{Electrogeneration flux} = 0 \\ \dfrac{d\Gamma_{III}}{dt} + \sum_{\forall\, reactions\ i} \nu_i r_i - \dfrac{I}{n\mathcal{F}} \times \dfrac{1}{S_{reaction\ area\ for\ 0<x<\mu}} = 0 \end{cases} \quad (25)$$

where: Γ_{III}: the Ni(III) surface concentration ($mol.m^{-2}_{electrode}$),

ν_i: the algebraic stochiometric constant of $Ni^{(III)}$ (dimensionless) of the chemical reaction i,

r_i: the rate ($mol.s^{-1}.m^{-2}_{electrode}$) of the chemical reaction i,

n: the number of electron transferred (dimensionless, here 1),

$\mathcal{F}$: the Faraday's constant,

$S_{reaction\ area\ for\ 0<x<\mu}$: the surface area of reaction (m^2).

Let's consider the following approximations:

(i) because the magnitude of the decreasing current after the plateau (due to the passivation) is smaller than 10 %, the maximum current can be considered to be the limiting current.

(ii) because a small value of scan rate is applied and a plateau is observed (*i.e.*, constant current at least for the first two temperatures), at each potential (in the range of 520 to 570 mV), the steady state is assumed to be reached for the nickel ($\frac{d\Gamma_{III}}{dt} = 0$).

Under these conditions, the rate of consumption of $Ni^{(III)}$ by the surface chemical reaction is equal to the electrogeneration flux, which leads to Eq. (26).

$$\sum_{\forall\ reactions\ i} \nu_i r_i = \frac{I}{n\mathcal{F}} \times \frac{1}{S_{reaction\ area\ for\ 0<x<\mu}} \quad (26)$$

Because the limitation of the current by the mass transfer of urea, this current can be expressed by Fick' first law as Eq. (27).

$$I_{max} = n\mathcal{F}DS_{reaction\ area\ for\ 0<x<\mu} \times \nabla C_{urea\ at\ the\ reaction\ area\ for\ 0<x<\mu} \quad (27)$$

It is not obvious how to determine the ∇C_{urea} at the reaction area for $0 < x < \mu$. For that, one can suppose that *(i)* since the plateau is reached (520 to 570 mV), this gradient is constant with temperature, and *(ii)* there is no limitation by internal diffusion (Knudsen).

Besides, the dependence of the diffusion coefficient on temperature may be expressed according to the Stokes-Einstein equation as Eq. (28) and illustrated in Fig. 9-b.

$$D = \frac{k_B T}{6\pi r \eta} \quad (28)$$

where: k_B: the Boltzmann constant (1.38×10^{-23} J.K^{-1}),

T: the absolute temperature (K),

r: the radius of the moving particle (r_{urea} calculated as 2.62×10^{-10} m [59]),

η: the viscosity (Pa.s).

The viscosity of the solutions of urea in alkaline medium has been measured, as presented in the Appendix A (see Fig. A.1). These values are used to calculate the diffusion coefficients.

Considering all these assumptions, equations and measurements, the Eqs. (29)-(30) are obtained:

$$\sum_{\forall\ reactions\ i} \nu_i r_i = \frac{I}{n\mathcal{F}S_{reaction\ area\ for\ 0<x<\mu}} = \nabla C_{reaction\ area\ for\ 0<x<\mu} \times D = constant \times D = constant \times \frac{k_B T}{6\pi r \eta} \quad (29)$$

$$I = constant \times \frac{T}{\eta} \quad (30)$$

The evolution of the current measured at the plateau as a function of the ratio T/η exhibits a linearity, expressed by Eq. (31) (R^2 = 0.993), confirming the validity of the assumption made and validating the proposed reaction scheme.

$$I_{max} = 0.012 \times T \quad (31)$$

In order to examine the temperature dependence of the diffusion coefficient *D*, we assume that it obeys to the Arrhenius' law, Eq. (32), and the logarithmic analysis of *D vs.* the reverse of *T* is performed:

$$D_{(T)} = D° \times \exp(-E_{a,d}/RT) \quad (32)$$

where: D_0: the diffusion coefficient when the temperature goes to infinity ($m^2.s^{-1}$),

$E_{a,d}$: the activation energy for diffusion ($J.mol^{-1}$).

The results, presented in inset of Fig. 9-b, lead to an activation energy for the urea diffusion $E_{a,d}$ of 21.2 $kJ.mol^{-1}$, close to the one obtained by Longsworth [60] (18.7 kJ. mol^{-1}).

With respect to the Eq. (29), an important question is to determine the reaction that consumes the nickel peroxide; indeed, since the oxidation of urea leads to byproducts (see next sections), it is obvious that several reaction intermediates consume $Ni^{(III)}$. One assumes here that only one reaction, r_χ, occurs (*i.e.*, the HCR) and that its rate can be expressed as Eq. (33).

$$r_{HCR} = k_{\chi(T)} \times \Gamma_{III}^{\beta} \times C_{OH^-}^{\gamma} \times C_{urea}^{\varepsilon} \quad (33)$$

where: $k_{\chi(T)}$: the reaction rate constant ($mol^{1-\beta-\gamma-\varepsilon}.m^{-2(1+\beta)+3(\gamma+\varepsilon)}.s^{-1}$),

β,γ,ε: the partial orders of reaction for nickel oxyhydroxide, hydroxide ion and urea respectively (dimensionless).

Consequently, the Eq. (26) can be written as Eq. (34).

$$I_{max\,(T)} = \left(n\mathcal{F}S_{reaction\ area\ for\ 0<x<\mu}\right) \times 6\, r_{HCR} = \left(n\mathcal{F}S_{reaction\ area\ for\ 0<x<\mu}\right) \times 6 \times k_{\chi(T)} \times \Gamma_{III}^{\beta} \times C_{OH^-}^{\gamma} \times C_{urea}^{\varepsilon} \quad (34)$$

Where 6 is the stochiometric factor of the $Ni^{(III)}$ in the HCR (dimensionless).

Assuming that the $k_{\chi(T)}$ obeys Arrhenius' law, the logarithmic analysis of the evolution of the current according to the equation Eq. (35) leads to the curve indicated in the inset in Fig. 9-a.

$$\ln\left(I_{max\,(T)}\right) = \ln\left(\mathcal{A}_{HCR} \times n\mathcal{F}S_{reaction\ area\ for\ 0<x<\mu} \times 6 \times r_{HCR}\right) - \frac{E_{a,HCR}}{RT} \quad (35)$$

where: $\mathcal{A}_{HCR}$: the pre-exponential factor,

$E_{a,HCR}$: the activation energy of the HCR ($J.mol^{-1}$).

Here, $E_{a,HCR}$ is estimated to be 49.3 kJ.mol^{-1}. The order of magnitude is substantially close to that of the oxidation of methanol on nickel electrode [61]. Note that this $E_{a,HCR}$ value is relatively low, which means that the reaction Eq. (13) between solid NiOOH and urea occurs easily, probably because the system is electrically activated during electrogeneration of NiOOH.

3.1.5. Dependence of the rate of rotation of the nickel electrode on the shape of the voltammogram curves for the electro-oxidation of urea

In this section, the effect on the obtained anodic current of the speed revolution of the nickel RDE is studied at two potential scan rates (0.83 and 5 mV.s^{-1}) and the obtained curves are illustrated in Fig. 10.

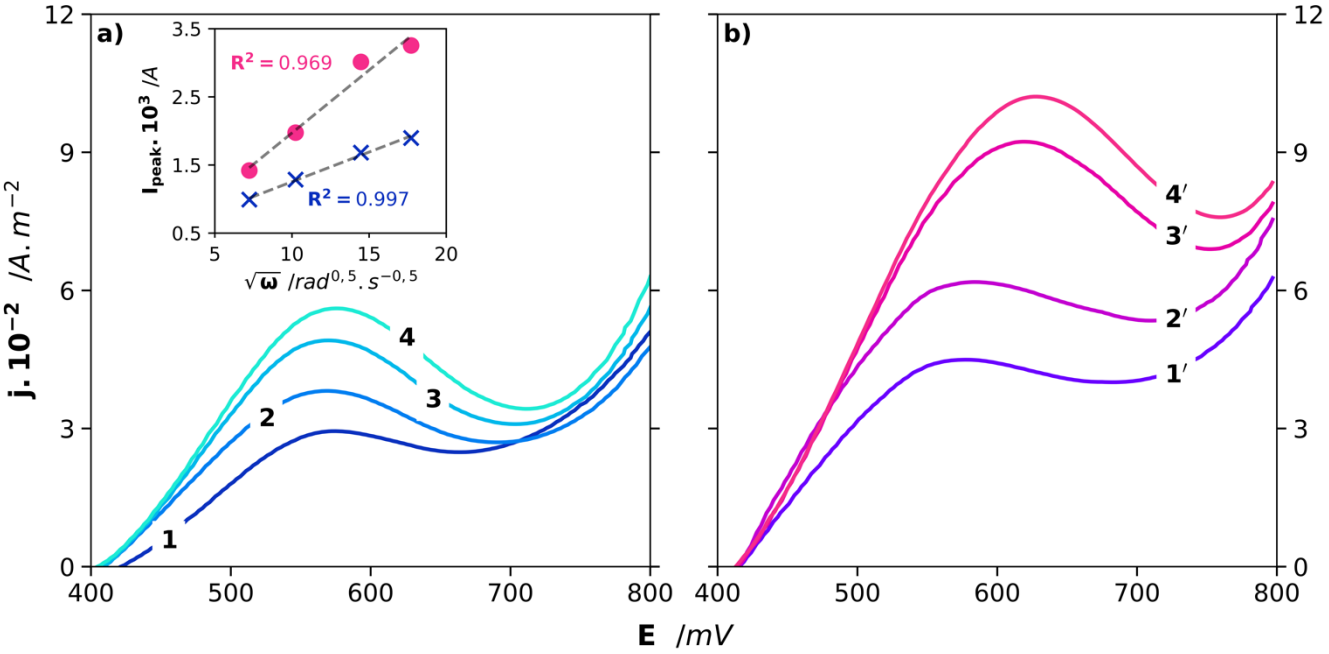

Fig. 10. Effect of the solution agitation on the shape of the current potential curves for the urea oxidation on nickel RDE (S = 3.14 mm^2) and at two potential scan rates: a) 0.83 mV.s^{-1} and b) 5 mV.s^{-1}. $[CO(NH_2)_2]_{t=0}$ = 0.33 mol.L^{-1}; [KOH] = 1 mol.L^{-1}; T = 298 K; Rotational speed of the RDE was 500 RPM (1-1'), 1000 RPM (2-2'), 2000 RPM (3-3') and 3000 RPM (4-4'). Inset shows the Levich plot at each scan rate 0.83 mV.s^{-1} (cross) and 5 mV.s^{-1} (dots).

Both potential scan rates are small enough to consider that at each applied potential, the system operates at steady state for NiOOH. The results shown in Fig. 10 highlight that in general, the current increases with the angular velocity of the RDE, ω, and the potential scan rate, ν. Furthermore, as ω and ν increase, the shape of the curves is deformed from a plateau to a peak.

Considering the curves obtained at the lowest stirring (500 RPM) for the two potential scan rates (0.83 and 5 $mV.s^{-1}$), both curves **1** and **1'** exhibit a pseudo plateau which, as before, is considered to indicate a limitation of mass transfer due to the diffusion of urea from the bulk to the HCR zone.

Indeed, recall that the anodic ER requires hydroxide anions. However, since the hydroxide concentration is in excess of the metallic nickel atoms, the current limitation is not due to the OH^- transfer to the anode. Besides, since both potential scan rates used are low, the time required for HCR to occur is sufficient, thus implying, for each applied potential, an immediate and continuous electrogeneration of NiOOH. Therefore, as the current increases, urea is consumed in the reaction zone ($0 < x < \mu$) and its concentration cancels, the plateau indicates a mass transfer limitation.

As the angular velocity increases (**1→2** and **1'→2'**), the current increases, which *(i)* reflects an increase of the urea diffusion flux arriving in the reaction zone ($0 < x < \mu$) and *(ii)* confirms the previous assumption made (i.e. there is no internal diffusion limitation ($0 < x < \mu$) (independent of the stirring) and thus only external diffusion limitation ($x > \mu$) is considered for the urea).

However, simultaneously with increasing current, the shape of the curves (520 to 650 mV) shifts from the plateau to the peak (a similar evolution is observed with temperature, in Fig. 9-a). The phenomenon is amplified for the highest ω studied (**2→4** and **2'→4'**). The same explanation as before is proposed, and due to this passivation phenomenon, the magnitude of the peak current could be smaller than the limiting current; therefore, although a linear evolution is observed between the current and the square root of the rate of rotation, the slopes of the straight lines are underestimated and the results are not analyzed according to the Levich' law.

3.2. Study of the indirect electro-oxidation of urea under potentiostatic electrolysis conditions

This first part of the study highlights the mediation of $Ni^{(II)}/Ni^{(III)}$ system to the urea oxidation and will serve as solid basis for further kinetic and mechanistic studies. The study emphasizes that there is no direct

oxidation of urea. Although the hydroxide ion concentration enhances the reversibility of the $Ni^{(II)}/Ni^{(III)}$ system, a trade-off is necessary to achieve a more environmentally sustainable process.

In a second set of experiences, preparative electrolysis, for which complete mass balances in liquid phase are systematically established, are performed, using undivided and divided electrochemical cells. In these experiments, particular attention is paid to make varying the concentrations of urea and KOH in a wide range and to be in excess of KOH over urea. The expected objective is to use all the significant data acquired, in order to select the optimal operating conditions, allowing *(i)* to reach a high degradation rate of urea and *(ii)* to reduce the electrogenerated adducts concentration more toxic than urea.

In this part, the objectives are twofold: *(i)* to identify and quantify the intermediates generated during the oxidation of urea in order to propose more accurate reaction pathways than the one given by the mineralization reaction of Eq. (13) *(ii)* to determine the optimal operating parameters in the perspective of designing a pilot capable of treating several liters of urea per day.

Electrolyzes are performed in potentiostatic mode since selective conditions are required. The applied potential (550 mV) is determined from voltammograms obtained in steady state (*i.e.*, at a potential scan rate of 0.83 $mV.s^{-1}$), in the case where the current reaches a limit value. As shown in Fig. 1, two cell configurations are used, either divided (anodic and cathodic compartments) or undivided. Aliquots of the electrolyzed solution are regularly collected and analyzed, following the methods described in the Experimental Section.

3.2.1. Identification of the electrogenerated adducts and mass balance on carbon and nitrogen elements

In order to identify the intermediate species generated during the UEO, an electrolysis is performed using mild operating conditions *i.e.*, room temperature, low alkalinity (1 $mol.L^{-1}$ of KOH) and an undivided cell. The results are summarized in Fig. 11 in the form of temporal (Fig. a), and even coulometric (Figs. b and c) evolution of the concentrations of the different species detected and analyzed.

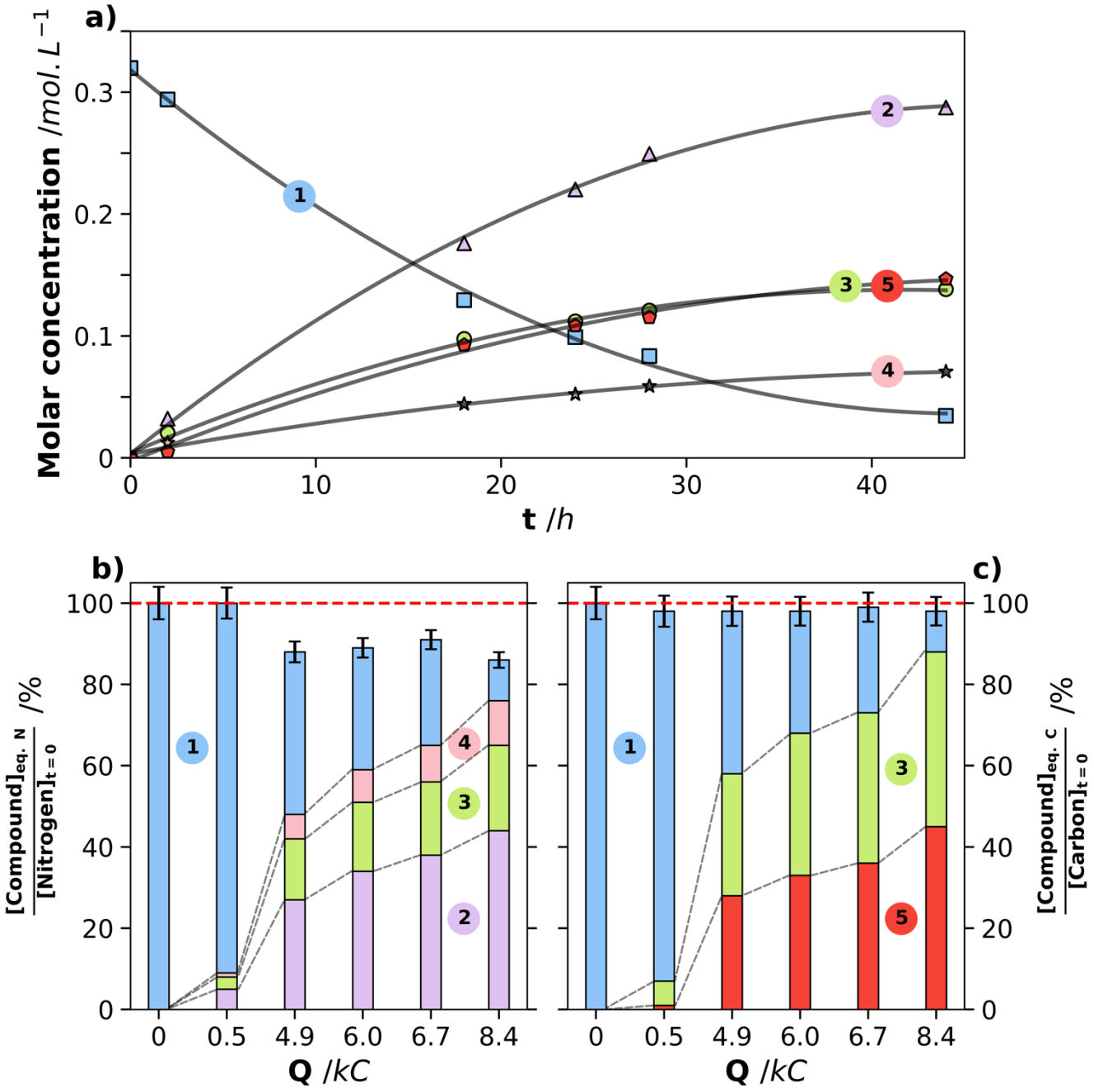

Fig. 11. Results of a typical potentiostatic preparative electrolysis on nickel electrode. S = 4 cm^2; [KOH] = 1.5 $mol.L^{-1}$; $[CO(NH_2)_2]_{t=0}$ = 0.33 $mol.L^{-1}$; $E_{applied}$ = 550 mV; T = 298 K; V = 50 mL. The graph a) shows the molar urea concentration profiles over the electrolysis time, as well as those for the obtained byproducts (the line curves are plotted with the aim of interpolating the concentration behavior, and thus do not correspond to modeling). The error bars in part a) are smaller than the size of labels and evaluated at 4%. The graph b) presents the nitrogen mass balance while the right part c) focuses on the carbon mass balance. The red dotted lines (in b) and c)) show a mass balance of 100%. The error bars represent the total error of the percentages. Labels : ①-□ $CO(NH_2)_2$, ②-△ NH_4^+, ③-○ OCN^-, ④-☆ NO_2^- and ⑤-◻ CO_3^{2-}.

Fig. 11-a) presents the time variation of the urea concentration (curve **1**) as well as the identified intermediates (curves **2** – **5**) generated during electrolysis.

As a first approximation, the evolution of urea concentration ($C_{urea_{(t)}}$) as a function of time is modeled by an apparent first-order kinetic model as Eq. (36).

$$C_{urea_{(t)}} = C^0_{urea} \times e^{-k_{app}t} \quad (36)$$

where: C^0_{urea}: the initial urea concentration (mol.L^{-1}),

k_{app}: the apparent rate constant of the HCR (s^{-1}).

Under these operating conditions, the value obtained for the constant rate k_{app} is 1.4×10^{-5} s^{-1}. In fact, an apparent 'first-order kinetic' constant describes the temporal evolution of an electroactive specie concentration (here the urea but also byproducts), present in a batch reactor, and subjected to potentiostatic electrolysis. Therefore, this simplest model does not elucidate neither the $\sum_{\forall\, reactions\, i} \nu_i r_i$ terms of the expression (29), nor the expression for the chemical rate of HCR.

Fig. 11-a also indicates the intermediates species identified into the liquid electrolyte, namely cyanate (OCN^-), nitrite (NO_2^-), carbonate (CO_3^{2-}) and NH_4^+ (in the ammonia form because the electrolyte is alkaline and pKa is equal to 9.25). Indeed, the ammonium form is obtained during the injection in the ion chromatography which leads to acidify the sample. Moreover, it should be noted that the formation of cyanate and carbonate occurs under equimolar conditions.

Fig. 11-b and c present the evolution, as a function of the amount of charge supplied, of the mass balances of total nitrogen (b) and total carbon (c) determined into the liquid electrolyte, and normalized by their respective initial quantities.

Fig. 11-c) highlights that, given the error bars, the carbon mass balance is quantitative at any instant of the electrolysis, meaning that all the disappearing urea is converted to CO_3^{2-} or OCN^-.

With respect to the nitrogen mass balance, Fig. 11-b) evidences that *(i)* the main nitrogen byproducts of urea oxidation in alkaline medium are in mineral form, NH_4^+ and NO_2^-, and in organic form, OCN^-, and *(ii)* these

byproducts accumulate over time. Moreover, ammonium remains the main species at more than 44 *mol%* at the end of the electrolysis.

While the mass balance of total carbon is almost quantitative, the mass balance of total nitrogen presents a deviation of up to 12% after 20 hours of electrolysis, and is therefore significant compared to the error bars. This can be explained in two ways. First, the uncertainty on the nitrogen is higher than on carbon, due to a larger number of nitrogen intermediates. Secondly, the gas phase has not been analyzed, and certainly contains nitrogen compounds such as N_2 or N_2O that may be stripped during the electrolysis.

In summary, under the chosen conditions, most of the urea oxidation products remain in the liquid phase and the gas produced (N_2 or N_2O), does not exceed 12% of the urea. This result is in agreement with the ones obtained by Li et al. [38], and Medvedev al. [62].

At this point, several pathways indicated by Eqs. (37)-(41), can be proposed in order to better understand the observed formation of byproducts at the Ni anode.

$$CO(NH_2)_2 \xrightarrow{\text{Ni catalyzed}} HOCN + NH_3 \quad (37)$$

$$HOCN + OH^- \xrightarrow{\text{Ni catalyzed}} OCN^- + H_2O \quad (38)$$

$$HOCN + 2OH^- \xrightarrow{\text{Ni catalyzed}} CO_3^{2-} + NH_3 \quad (39)$$

$$NH_3 + 7OH^- \xrightarrow{\text{Ni catalyzed}} NO_2^- + 5H_2O + 6e^- \quad (40)$$

$$OCN^- + 8OH^- \xrightarrow{\text{Ni catalyzed}} NO_2^- + CO_3^{2-} + 4H_2O + 6e^- \quad (41)$$

where: 1 e^- represents one reduction of NiOOH to $Ni(OH)_2$.

It has been verified that during the same duration of the experiments, without external energy input, no conversion of urea or formation of byproducts is observed, which excludes the assumption of a ‘natural’ hydrolysis of urea.

3.2.2. Influence of the presence (or not) of the ionic separator (undivided cell vs divided cell)

The use of a membrane as separator introduces an ohmic drop, and thus induces an increase in energy consumption, in addition to its relatively high cost and the possible risks of its poisoning by organic compounds [63,64]. The H-shaped electrochemical cell, described in Fig. 1, is used with or without separator; in fact, due to its geometric shape, it enables an easy separation of the cathodic electrogenerated hydrogen, avoiding its oxidation in the anodic compartment [18]. The following section is devoted to the study of the impact of the separator on the mechanism path, the nature and concentration of electrogenerated adducts. As mentioned above, the volume chosen for the anolyte (for electrolysis with a membrane) is the same as the volume of the electrolyte in the case of no membrane.

Fig. 12 presents the mass balances in the liquid phase, for electrolysis carried out with (circles) and without (triangles) membrane. Figs 12 a to f indicate the evolution, against the amount of charge supplied, of the concentrations of urea, cyanate, ammonium, nitrite, total N and total C, respectively, normalized by the initial urea concentration. The repeatability of the experiments is checked by performing each electrolysis twice.

As shown in Fig. 12-a, the presence of an ionic separator has no impact on the conversion rate of urea during electrolysis. This result is important because it shows that urea is not reducible and that there is no hydrogen produced at the cathode that oxidizes at the anode.

Figs 12 b and c, indicate similar results for cyanate and ammonium respectively. Indeed, an almost perfect overlap of the experimental points can be observed for both conditions, which means that the formation of cyanate and ammonium ions is not affected by the presence of the membrane. Similar conclusions to the previous ones can be made: none of these species reduces at the cathode.

Conversely, a different behavior is observed for nitrites, plotted in Fig. 12-d, whose concentration, at equivalent amount of charge supplied, is decreased by more than two times in the absence of membrane, which means that nitrites are reduced at the Pt cathode [65]. The products related to the nitrite reduction

have not been detected in the liquid electrolyte, so the formation of gaseous products, degassed during electrolysis, would be privileged. It should be noted that a quantitative analysis of the gas phase will be considered in a future study.

Despite uncertainties, the balance on the carbon element, Fig. 12-f, appears to be quantitative. The deviations are larger in the case of the nitrogen balance, Fig. 12-e. However, one cannot know whether significant amounts of N_2 are produced or not.

These results show that in the absence of a membrane separator, electrolysis leads to lower amounts of nitrite, without impacting the concentration of other compounds which means that the product of this reduction should be formed in low concentration and degassed during electrolysis. As a consequence, the use of an undivided cell is interesting as it avoids the issues related to technological complexity, increased ohmic drop, as well as fouling of the membrane surface. However, it should be kept in mind that, for an equivalent amount of charge supplied, such undivided configuration reduces the amount of nitrite but also the amount of hydrogen formed at the cathode. With regard to the prospect of a larger scale process, the application of a potential may allow a better control of byproducts formation, compared to galvanostatic electrolysis. Indeed, at higher potentials, oxidation of nitrite to nitrate has been observed [38].

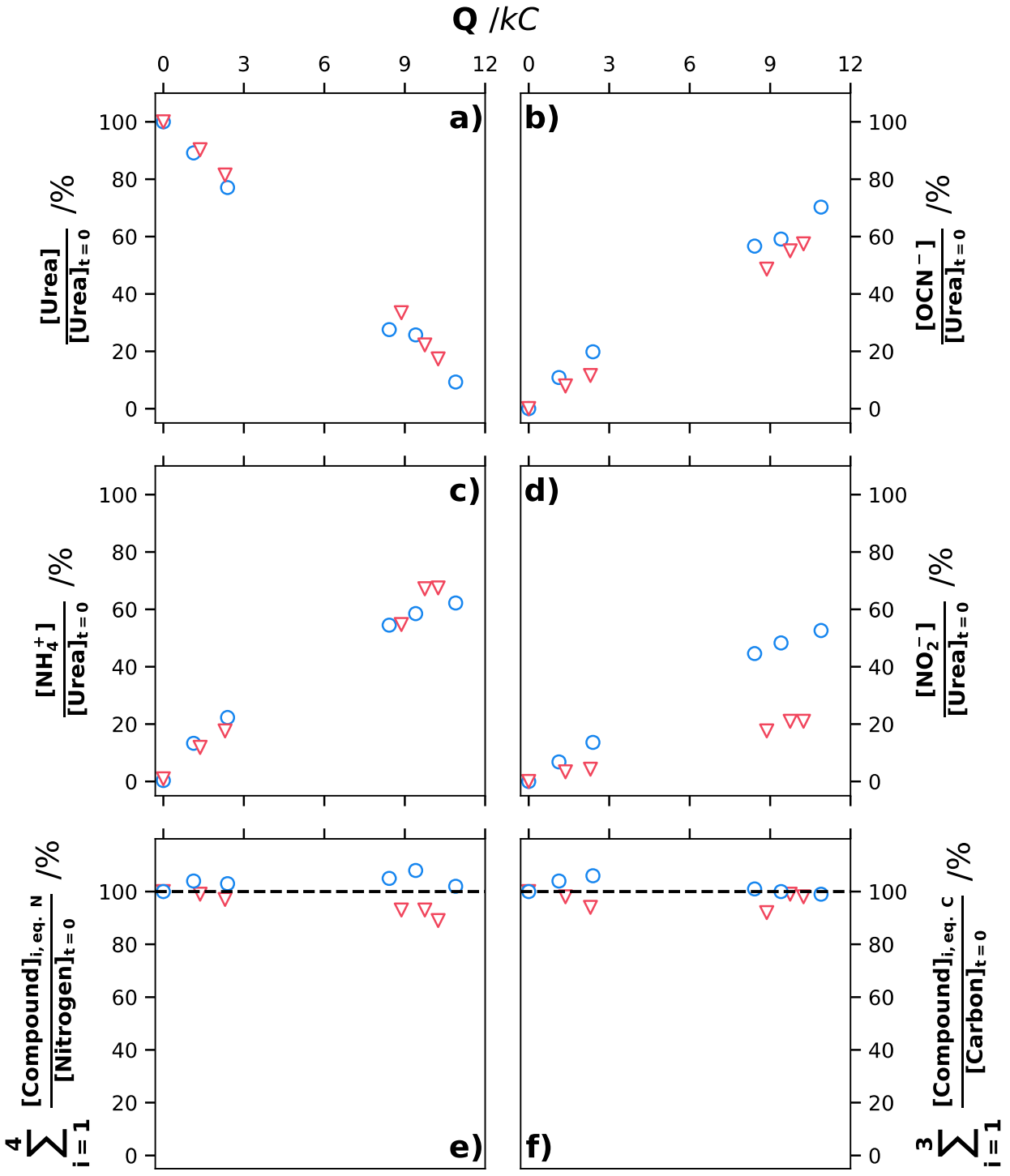

Fig. 12. Results of an indirect electro-oxidation of the urea carried out in a H-shaped electrochemical cell (cell c) in Fig. 1). $E_{applied}$ = 550 mV; T = 298 K; $[CO(NH_2)_2]_{t=0}$ = 0.33 mol.L^{-1}; [KOH] = 2 mol.L^{-1}; S = 15.7 cm^2; V = 70 mL. The results are presented as the evolution of the normalized concentration of the various products against the amount of supplied charge. Urea, cyanate, ammonium and nitrite are represented, respectively, in part a), b), c) and d). The nitrogen mass balance, e), and carbon balance, f), are normalized in initial concentration. Uncertainties are lower than 4.6 %. Circles correspond to the experiments carried out with a membrane. Triangles correspond to the experiments carried out without a membrane.

3.2.3. Influence of the alkalinity

Potassium hydroxide is a strong base and remains a corrosive and toxic reagent whose use should be limited (or even avoided) especially in a wastewater treatment perspective. However, the preliminary study of voltammograms have shown that KOH contributes to increase the rate of the overall process (hydroxide ions are needed for the ER (Eq. (12)) and the HCR (Eq. (13)). Consequently, a compromise has to be found in order to operate with the minimum KOH required for avoiding additional environmental problems and of course for minimizing the cost of the electrolysis. Its influence on the urea oxidation products is studied in this sub-section, varying the concentration in a wide range (1 to 5 mol.L^{-1}).

Fig. 13-a shows that urea conversion, independent of the KOH concentration, can reach values of 90 %. For an equivalent amount of charge supplied, even though the overall process increases with the KOH concentration, the urea conversion is unimpacted. A similar evolution is observed with the other byproducts (ammonium and cyanate, respectively, Figs. b and c) where their compositions are not affected by the KOH concentration (in the range of 1 to 5 mol.L^{-1}). The final concentration of nitrite (~20 *mol%*) is identical to that in the previous sub-section (without membrane) for the same amount of charge supplied. However, some differences appear for urea conversion above 80%. Note that the amount of ammonium obtained corresponds to the same amount of urea oxidized, meaning that one nitrogen of the urea leads to one nitrogen of ammonium. The other nitrogen of the urea is transformed to cyanate, nitrite and probably N_2 gas. Comparatively to the previously used H-shaped undivided cell (*i.e.*, Fig. 12), the cell used here (Metrohm type undivided cell) present a more efficient mixing efficiency at the anode and to a lesser extent, at the cathode (because the hydrogen evolution), thus implying an increase of the mass transfer of *(i)* an electroactive species going to the electrode or *(ii)* any species going to the active area ($0 < x < \mu$) to be adsorbed. Therefore, the rate of the corresponding process is higher in the Metrohm type cell compared to the H shaped cell. Comparing the final concentrations of cyanate and ammonium, obtained from the electrolysis performed in cell-c), with the final concentrations, obtained from the electrolysis carried out in cell-b), one can observe a decrease of 20 *mol%* and a 40 *mol%* increase in concentration at equivalent

amount of charge supplied of cyanate and ammonium respectively. This behavior appears to be consisted with stirring-promoted pathways suggested in Eqs. (37)-(41).

Fig. 13-f confirms that the carbon mass balance is close to 100 % regardless of KOH concentration. As shown in Fig. 13-e, the mass balance of nitrogen presents a deviation that tends to increase during electrolysis, with a maximum of 20 % after 45 hours of electrolysis. Such a deviation would suggest that nitrogen gas is produced.

In summary, the KOH concentration has no impact on byproduct production and composition; increasing its concentration has the advantage of reducing the electrolysis time, but using concentrated alkaline solution remains difficult to recycle. A compromise must be found for larger scale operation.

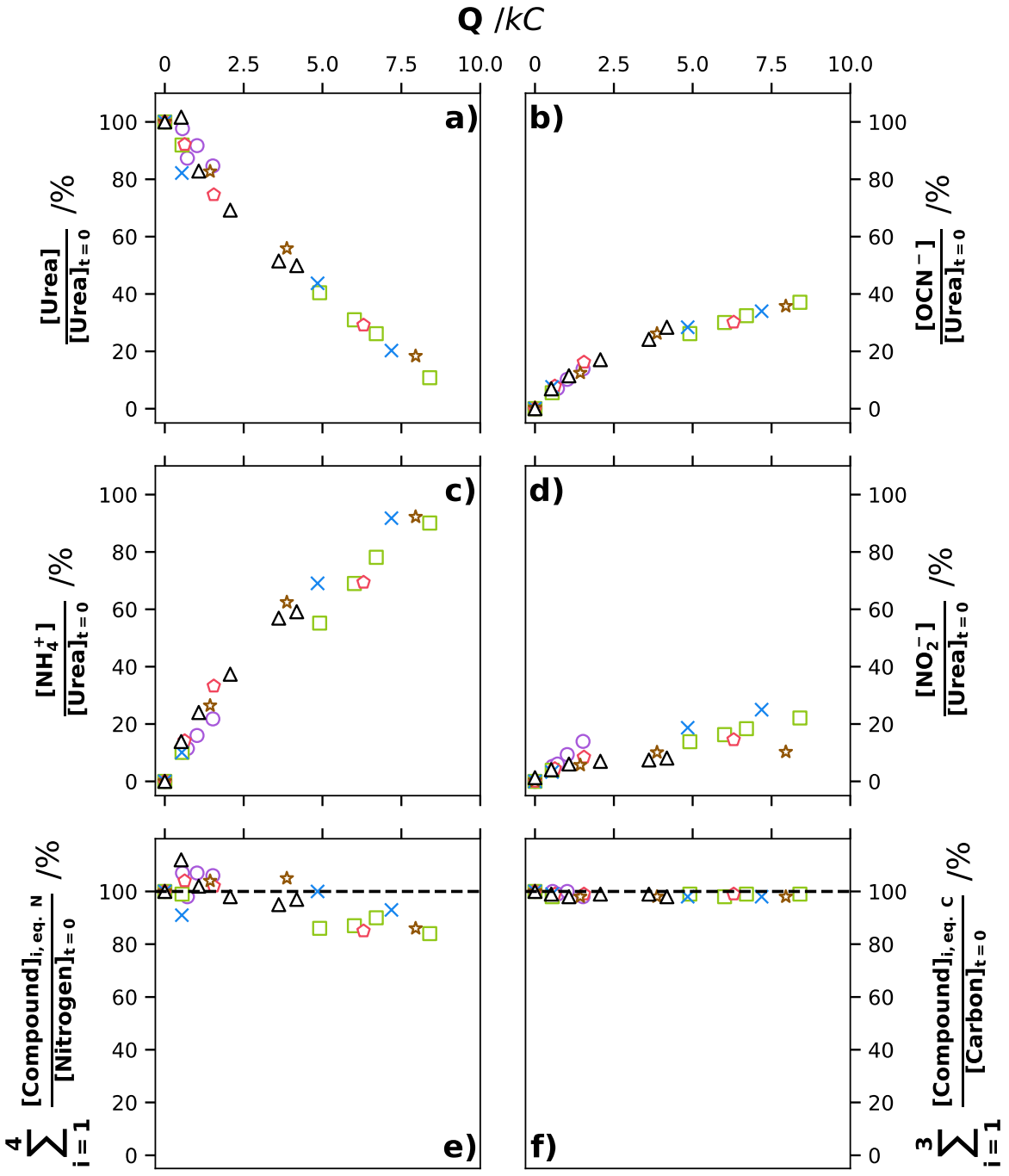

Fig. 13. Results of an indirect electrooxidation of urea in a stirred undivided cell (Metrohm type cell, represented by cell b) in Fig. 1) using various KOH concentration. $E_{applied}$ = 550 mV; T = 298 K; $[CO(NH_2)_2]_{t=0}$ = 0.33 mol.L^{-1}.; S = 4 cm^2; V = 50 mL; stirred by magnetic bar (ω = 500 RPM, length of the bar: 2 cm; diameter of the bottom area of the cell: 4 cm). The results are presented as the evolution of the normalized concentration of the different byproducts as a function of the amount of supplied charge. Urea, cyanate, ammonium, and nitrite are shown in parts (a), (b), (c), and (d), respectively. The nitrogen mass balance, e), and carbon mass balance, f), are normalized with respect to the initial concentration. The KOH concentrations used are ◯ 1, ▢ 1.5, ▯ 2.5, × 3, ☆ 4, and △ 5 mol.L^{-1}.The uncertainties are smaller than 5.1%.

3.2.4. Influence of the temperature

Temperature is a parameter affecting the rate of chemical reactions of the HCR and those of Eqs. (37)-(41) as well as the diffusion coefficient of urea. So theoretically, it positively impacts the overall rate of urea

oxidation, even if, in the perspective of the process development at pilot scale, it would induce higher operating cost. The influence of the temperature on urea oxidation is carried out at various temperatures (ranging 293 to 313 K), and the results are presented in the Fig. 14, giving the composition of the different adducts as a function of the amount of charge supplied. The electrolysis times result in nearly complete urea conversions (~ 90 %) for all the operating temperatures. Note that because temperature causes an increase in anodic current (at constant potential) (Fig. 14-g), the electrolyzes durations decrease as the temperature increases.

The profiles of normalized concentrations of urea, cyanate, ammonium and nitrite as a function of amount of charge supplied (Figs 14 a, b, c and d, respectively) appear similar regardless of the temperature ranging from 293 to 313 K (this indirectly validates the relatively low value of the activation energy, determined previously).

At the same amount of charge supplied, the concentrations of urea and byproducts are similar to those obtained in the previous sub-section, meaning that neither KOH concentration nor temperature significantly affects the reaction pattern of urea oxidation. Nitrite formation is not impacted by temperature.

The total mass balances exhibit the same behavior as in the previous sub-sections: the carbon balance (Fig. f), is close to 100 % and, conversely, the balance of nitrogen compounds (Fig. e) shows losses, which increase as a function of the amount of charge supplied (*i.e.,* duration of electrolysis) and should correspond to the gas produced (up to about 20 %).

Fig. 14-g evidences the resulting current profiles as a function of time. The decrease in current is not related to any passivation but to the direct decrease in urea concentration in the bulk (urea conversions reach 90 %). In the same way as when KOH concentration is increased, the increase of temperature leads to:

(i) an increase in the current magnitude, due to the increase in both the urea diffusion coefficient and the kinetic constant of HCR.

(ii) a more pronounced decrease in current due to the more rapid decrease in urea concentration.

In brief, the increase of temperature allows to go faster and reduce the electrolysis time against an additional energy input for heating. In view of these results, the use of a heated reactor is not required in a scale-up perspective.

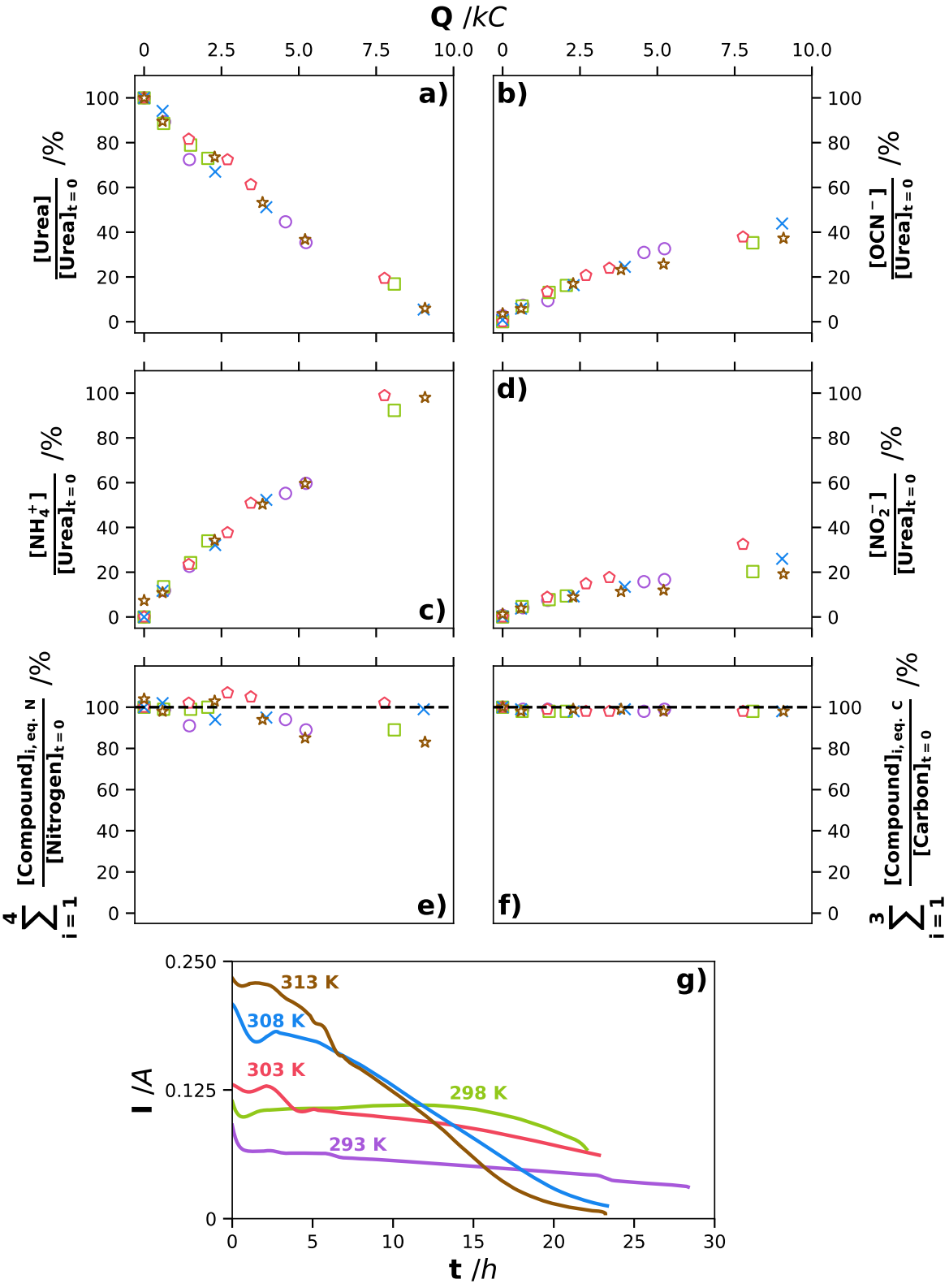

Fig. 14. Results of an indirect electrooxidation of urea in a stirred undivided cell (Metrohm type cell, represented as cell b) in Fig. 1) using various temperature. $E_{applied}$ = 550 mV; $[CO(NH_2)_2]_{t=0}$ = 0.33 mol.L^{-1}; [KOH] = 2 mol.L^{-1}; S = 4 cm^2; V = 50 mL. The results are presented as the evolution of the normalized concentration of the different byproducts as a function of the amount of charge supplied. Urea, cyanate, ammonium, and nitrite are shown in parts (a), (b), (c), and (d), respectively. The nitrogen mass balance, e), and carbon balance, f), are normalized with respect to initial concentration. The temperatures are ◯ 293, ▢ 298, ▯ 303, × 308 and ☆ 313 K. The uncertainties are smaller than 5.9 %. The current profiles over the electrolysis time are presented in part g).

4. Conclusions

In this work, the urea electro-oxidation (UEO) in alkaline media was intensively investigated at laboratory-scale.

First, the results provided evidence for the mediation of the $Ni^{(II)}/Ni^{(III)}$ system in urea oxidation via the decoupling of $Ni^{(II)}$ electro-oxidation step (upper to 5 mV.s^{-1}) from the indirect heterogeneous urea oxidation (lower to 5 mV.s^{-1}), creating a consistent context for further kinetic and mechanistic study. By introducing the Turn Over Number (TON), the study demonstrated that no direct urea oxidation occurred. The hydroxide ion concentration strongly influenced the reversibility of the $Ni^{(II)}/Ni^{(III)}$ system. Towards more environmentally sustainable process, decreasing this concentration, at least to 1 mol.L^{-1} seems to be a relevant strategy. From the analysis of the viscosities, the urea diffusion coefficient was determined as well as the corresponding activation energy from the voltammograms.

Secondly, laboratory-scale electrolyzes were carried out with urea conversions close to 90 %, contrary to most of the published works. By implementing various analytical methods, mass balances in the liquid phase could be established; while they were found complete for the carbon element, they deviated by up to 20% for the nitrogen element, showing that some gaseous compounds should be produced. Another original result was the identification of the cyanate, ammonium, nitrite, and carbonate ions as the major byproducts of UEO. In the perspective of larger scale implementing UEO, the amount of these by-products had to be reduced in order to orientate the mineralization of urea towards non-polluting compounds. Experiments performed in a mono-compartment cell configuration showed that nitrites could be reduced at the cathode, thereby reducing the amount of environmentally harmful byproducts by 50 %, but at the expense the production of hydrogen. Furthermore, by varying from 293 to 313 K, the temperature of the reactional medium had no influence on the formation of byproducts. From an environmental process perspective, it

would be interesting to perform a mass balance on the nickel electrode in order to exclude any pollution due to nickel release.

From this work, some guidelines could be proposed in order to design and operate an electrolyzer able to treat urea by this electrochemical method. They would consist in implementing an undivided cell configuration, containing an electrolyte with 1 $mol.L^{-1}$ KOH and at room temperature.

Nomenclature

Latin letters

- $\mathcal{A}_{HCR}$: pre-exponential factor of the HCR
- C_i : molar concentration of the constituent i ($mol.L^{-1}$)
- D_i: diffusion coefficient of the constituent i ($m^2.s^{-1}$)
- D_0: diffusion coefficient when the temperature reaches infinity ($m^2.s^{-1}$)
- E: applied potential (mV)
- E°: standard potential (mV)
- $E_{I=0}$: open circuit potential (mV)
- $E_{a,HCR}$: activation energy for the HCR processus ($J.mol^{-1}$)
- $E_{a,d}$: activation energy for diffusion ($J.mol^{-1}$)
- $\mathcal{F}$: Faraday's constant (96 500 $C.mol^{-1}$)
- I: current (A)
- j: current density ($A.m^{-2}$)
- k_{app} : apparent rate constant of the HCR (s^{-1})
- r_χ: superficial chemical reaction rate ($mol.m^{-2}.s^{-1}$)
- Q: amount of charge supplied to the system (C)
- S: electrode surface area (m^2)
- t: electrolysis time (h)
- T: temperature (K)
- V: electrolyte volume (m^3)

Greek letters

- Γ_i: superficial concentration of the specie i ($mol.m^{-2}$)
- η: dynamic viscosity (Pa.s)
- ν_{scan}: scan rate ($V.s^{-1}$)
- ρ: specific gravity ($kg.m^{-3}$)
- ω: angular velocity ($rad.s^{-1}$)

Abbreviations

- CE: counter (or auxiliary) electrode
- ER: electrogenerated reaction
- HCR: heterogeneous catalytic reaction
- IC: inorganic carbon ($g.L^{-1}$)
- NPOC: non purgeable organic carbon ($g.L^{-1}$)
- POC: purgeable organic carbon ($g.L^{-1}$)
- RDE: rotating disk electrode
- RPM: rounds per minute ($tr.min^{-1}$)
- SCE: saturated calomel electrode
- SHE: standard hydrogen electrode
- TON: turn over number
- UEO : urea electro-oxidation
- WE : working electrode

Acknowledgements

This work was supported by the French National Research Agency (proposal HYUREA ANR-19-CE04-0009). The authors gratefully acknowledged the partners of this proposal for their helpful discussion, especially Pr. C. Cachet Vivier, Dr. S. Bastide, Dr. C. M. Sánchez-Sánchez and Dr. V. Vivier.

5. References

[1] S.E. Vollset, E. Goren, C.-W. Yuan, J. Cao, A.E. Smith, T. Hsiao, C. Bisignano, G.S. Azhar, E. Castro, J. Chalek, A.J. Dolgert, T. Frank, K. Fukutaki, S.I. Hay, R. Lozano, A.H. Mokdad, V. Nandakumar, M. Pierce, M. Pletcher, T. Robalik, K.M. Steuben, H.Y. Wunrow, B.S. Zlavog, C.J.L. Murray, Fertility, mortality, migration, and population scenarios for 195 countries and territories from 2017 to 2100: a forecasting analysis for the Global Burden of Disease Study, The Lancet. (2020). https://doi.org/10.1016/S0140-6736(20)30677-2.

[2] U. Badeti, N.K. Pathak, F. Volpin, U. Dorji, S. Freguia, H.K. Shon, S. Phuntsho, Impact of source-separation of urine on effluent quality, energy consumption and greenhouse gas emissions of a decentralized wastewater treatment plant, Process Safety and Environmental Protection. (2021). https://doi.org/10.1016/j.psep.2021.04.022.

[3] D.F. Putnam, Composition and Concentrative Properties of Human Urine, National Aeronautics and Space Administration, 1971. http://ntrs.nasa.gov/archive/nasa/casi.ntrs.nasa.gov/19710023044_1971023044.pdf.

[4] E.N. Taylor, G.C. Curhan, Body Size and 24-Hour Urine Composition, American Journal of Kidney Diseases. (2006). https://doi.org/10.1053/j.ajkd.2006.09.004.

[5] K. Mahalik, J.N. Sahu, A.V. Patwardhan, B.C. Meikap, Kinetic studies on hydrolysis of urea in a semi-batch reactor at atmospheric pressure for safe use of ammonia in a power plant for flue gas conditioning, Journal of Hazardous Materials. (2010). https://doi.org/10.1016/j.jhazmat.2009.10.053.

[6] Y. Qin, J.M.S. Cabral, Review Properties and Applications of Urease, Biocatalysis and Biotransformation. (2002). https://doi.org/10.1080/10242420210154.

[7] A. Muhammad Yusuf., F. Mulana, S.D. Said, Effects of ultraviolet-enhanced ozonation on the degradation of ammonia and urea in fertilizer plant wastewater, IOP Conference Series: Materials Science and Engineering. (2019). https://doi.org/10.1088/1757-899X/536/1/012079.

[8] T. Kameda, S. Ito, T. Yoshioka, Kinetic and equilibrium studies of urea adsorption onto activated carbon: Adsorption mechanism, Journal of Dispersion Science and Technology. (2017). https://doi.org/10.1080/01932691.2016.1219953.

[9] B. Koubaissy, J. Toufaily, Z. Yaseen, T.J. Daou, S. Jradi, T. Hamieh, Adsorption of uremic toxins over dealuminated zeolites, Adsorption Science & Technology. (2017). https://doi.org/10.1177/0263617416666084.

[10] A.M. Bernhard, D. Peitz, M. Elsener, T. Schildhauer, O. Kröcher, Catalytic urea hydrolysis in the selective catalytic reduction of NOx : catalyst screening and kinetics on anatase TiO_2 and ZrO_2, Catalyst. Science Technology. (2013). https://doi.org/10.1039/C2CY20668D.

[11] G. Lourinho, P.S.D. Brito, Electrolytic Treatment of Swine Wastewater: Recent Progress and Challenges, Waste Biomass Valor. (2021). https://doi.org/10.1007/s12649-020-00951-4.

[12] S.G. Simoes, J. Catarino, A. Picado, T.F. Lopes, S. Di Berardino, F. Amorim, F. Gírio, C.M. Rangel, T. Ponce de Leão, Water availability and water usage solutions for electrolysis in hydrogen production, Journal of Cleaner Production. (2021). https://doi.org/10.1016/j.jclepro.2021.128124.

[13] A. Kapałka, G. Fóti, C. Comninellis, Basic Principles of the Electrochemical Mineralization of Organic Pollutants for Wastewater Treatment, in: C. Comninellis, G. Chen (Eds.), Electrochemistry for the Environment, Springer, 2010: pp. 1–23. https://doi.org/10.1007/978-0-387-68318-8_1.

[14] M. Jafari, G.G. Botte, Electrochemical treatment of sewage sludge and pathogen inactivation, Journal of Applied Electrochemistry. (2021). https://doi.org/10.1007/s10800-020-01481-6.

[15] J.F. Patzer, S.J. Yao, S.K. Wolfson, Platinized-titanium electrodes for urea oxidation Part I. Demonstration of efficacy, Journal of Molecular Catalysis. (1991). https://doi.org/10.1016/0304-5102(91)80163-W.

[16] M. Cataldo Hernández, N. Russo, M. Panizza, P. Spinelli, D. Fino, Electrochemical oxidation of urea

in aqueous solutions using a boron-doped thin-film diamond electrode, Diamond and Related Materials. (2014). https://doi.org/10.1016/j.diamond.2014.02.006.

[17] B.K. Boggs, R.L. King, G.G. Botte, Urea electrolysis: direct hydrogen production from urine, Chemical Communications. (2009). https://doi.org/10.1039/b905974a.

[18] Z. Zhou, Y. Liu, J. Zhang, H. Pang, G. Zhu, Non-precious nickel-based catalysts for hydrogen oxidation reaction in alkaline electrolyte, Electrochemistry Communications. (2020). https://doi.org/10.1016/j.elecom.2020.106871.

[19] J. Li, S. Wang, J. Chang, L. Feng, A review of Ni based powder catalyst for urea oxidation in assisting water splitting reaction, Advanced Powder Materials. (2022). https://doi.org/10.1016/j.apmate.2022.01.003.

[20] D. Wang, G.G. Botte, In Situ X-Ray Diffraction Study of Urea Electrolysis on Nickel Catalysts, ECS Electrochemistry Letters. 3 (2014) H29–H32. https://doi.org/10.1149/2.0031409eel.

[21] V. Vedharathinam, G.G. Botte, Direct evidence of the mechanism for the electro-oxidation of urea on $Ni(OH)_2$ catalyst in alkaline medium, Electrochimica Acta. (2013). https://doi.org/10.1016/j.electacta.2013.06.137.

[22] R.K. Singh, P. Subramanian, A. Schechter, Enhanced Urea Activity of Oxidation on Nickel-Deposited Tin Dendrites, ChemElectroChem. (2017). https://doi.org/10.1002/celc.201600862.

[23] D.A. Daramola, D. Singh, G.G. Botte, Dissociation Rates of Urea in the Presence of NiOOH Catalyst: A DFT Analysis, The Journal of Physical Chemistry. (2010). https://doi.org/10.1021/jp105159t.

[24] V. Vedharathinam, G.G. Botte, Experimental Investigation of Potential Oscillations during the Electrocatalytic Oxidation of Urea on Ni Catalyst in Alkaline Medium, J. Phys. Chem. C. 118 (2014) 21806–21812. https://doi.org/10.1021/jp5052529.

[25] R.K. Singh, A. Schechter, Electrochemical investigation of urea oxidation reaction on β-$Ni(OH)_2$ and $Ni/Ni(OH)_2$, Electrochimica Acta. (2018). https://doi.org/10.1016/j.electacta.2018.05.049.

[26] F. Guo, K. Ye, M. Du, X. Huang, K. Cheng, G. Wang, D. Cao, Electrochemical impedance analysis of urea electro-oxidation mechanism on nickel catalyst in alkaline medium, Electrochimica Acta. (2016).

https://doi.org/10.1016/j.electacta.2016.05.149.

[27] S. Chakrabarty, I. Offen-Polak, T.Y. Burshtein, E.M. Farber, L. Kornblum, D. Eisenberg, Urea oxidation electrocatalysis on nickel hydroxide: the role of disorder, Journal of Solid State Electrochemistry. (2020). https://doi.org/10.1007/s10008-020-04744-6.

[28] N.A.M. Barakat, M.H. El-Newehy, A.S. Yasin, Z.K. Ghouri, S.S. Al-Deyab, Ni&Mn nanoparticles-decorated carbon nanofibers as effective electrocatalyst for urea oxidation, Applied Catalysis A: General. (2016). https://doi.org/10.1016/j.apcata.2015.11.015.

[29] R. Ding, L. Xudong, S. Wei, X. Qilei, W. Luo, J. Haixia, Y. Zeng, L. Enhui, Mesoporous Ni-P nanocatalysts for alkaline urea electrooxidation, Electrochimica Acta. (2016). https://doi.org/10.1016/j.electacta.2016.10.198 0013-4686/ã 2016 Elsevier Ltd. All rights reserved.

[30] R. Ding, L. Qi, M. Jia, H. Wang, Facile synthesis of mesoporous spinel $NiCo_2O_4$ efficient electrocatalysts for urea electro-oxidation, Nanoscale. (2014). https://doi.org/10.1039/C3NR05359H.

[31] W. Simka, J. Piotrowski, G. Nawrat, Influence of anode material on electrochemical decomposition of urea, Electrochimica Acta. (2007). https://doi.org/10.1016/j.electacta.2006.12.017.

[32] C.. B. Sun, M.W. Guo, S.S. Siwal, Q.B. Zhang, Efficient hydrogen production via urea electrolysis with cobalt doped nickel hydroxide-riched hybrid films: Cobalt doping effect and mechanism aspect, Journal of Catalysis. (2020). https://doi.org/10.1016/j.jcat.2019.11.034.

[33] W. Yan, D. Wang, G.G. Botte, Electrochemical decomposition of urea with Ni-based catalysts, Applied Catalysis B: Environmental. 127 (2012) 221–226. https://doi.org/10.1016/j.apcatb.2012.08.022.

[34] K. Ye, D. Zhang, F. Guo, K. Cheng, G. Wang, D. Cao, Highly porous nickel@carbon sponge as a novel type of three-dimensional anode with low cost for high catalytic performance of urea electro-oxidation in alkaline medium, Journal of Power Sources. (2015). https://doi.org/10.1016/j.jpowsour.2015.02.149.

[35] L. Wang, T. Du, J. Cheng, X. Xie, B. Yang, M. Li, Enhanced activity of urea electrooxidation on nickel catalysts supported on tungsten carbides/carbon nanotubes, Journal of Power Sources. (2015). https://doi.org/10.1016/j.jpowsour.2015.01.141.

[36] E. Urbańczyk, Urea removal from aqueous solutions—a review, Journal of Applied

Electrochemistry. (2016). https://doi.org/10.1007/s10800-016-0993-6.

[37] R.K. Singh, K. Rajavelu, M. Montag, A. Schechter, Advances in Catalytic Electrooxidation of Urea: A Review, Energy Technology. (2021). https://doi.org/10.1002/ente.202100017.

[38] J. Li, J. Li, T. Liu, L. Chen, Y. Li, H. Wang, X. Chen, M. Gong, Z. Liu, X. Yang, Deciphering and Suppressing Over- Oxidized Nitrogen in Nickel- Catalyzed Urea Electrolysis, Angewandte Chemie International Edition. (2021). https://doi.org/10.1002/anie.202107886.

[39] R.A. Nickell, W.H. Zhu, R.U. Payne, D.R. Cahela, B.J. Tatarchuk, Hg/HgO electrode and hydrogen evolution potentials in aqueous sodium hydroxide, Journal of Power Sources. (2006). https://doi.org/10.1016/j.jpowsour.2006.05.028.

[40] L. Liu, H. Mo, S. Wei, D. Raftery, Quantitative analysis of urea in human urine and serum by ^{1}H nuclear magnetic resonance, The Analyst. (2012). https://doi.org/10.1039/C2AN15780B.

[41] A. Seghiouer, J. Chevalet, A. Barhoun, F. Lantelme, Electrochemical oxidation of nickel in alkaline solutions: a voltammetric study and modelling, Journal of Electroanalytical Chemistry. (1998). https://doi.org/10.1016/S0022-0728(97)00498-1.

[42] W. Visscher, E. Barendrecht, The anodic oxidation of nickel in alkaline solution, Electrochimica Acta. (1980). https://doi.org/10.1016/0013-4686(80)87072-1.

[43] V. Vedharathinam, G.G. Botte, Understanding the electro-catalytic oxidation mechanism of urea on nickel electrodes in alkaline medium, Electrochimica Acta. (2012). https://doi.org/10.1016/j.electacta.2012.07.007.

[44] C. Costentin, S. Drouet, M. Robert, J.-M. Savéant, Turnover Numbers, Turnover Frequencies, and Overpotential in Molecular Catalysis of Electrochemical Reactions. Cyclic Voltammetry and Preparative-Scale Electrolysis, Journal of the American Chemical Society. (2012). https://doi.org/10.1021/ja303560c.

[45] P.K.T. Nguyen, J. Kim, Y.S. Yoon, H.H. Yoon, J. Hur, Mathematical modeling of a direct urea fuel cell, International Journal of Hydrogen Energy. 48 (2023) 2314–2327. https://doi.org/10.1016/j.ijhydene.2022.10.052.

[46] R. Lin, L. Kang, T. Zhao, J. Feng, V. Celorrio, G. Zhang, G. Cibin, A. Kucernak, D.J.L. Brett, F.

Corà, I.P. Parkin, G. He, Identification and manipulation of dynamic active site deficiency-induced competing reactions in electrocatalytic oxidation processes, Energy & Environmental Science. (2022). https://doi.org/10.1039/D1EE03522C.

[47] S. Wang, P. Xu, J. Tian, Z. Liu, L. Feng, Phase structure tuning of graphene supported Ni-NiO Nanoparticles for enhanced urea oxidation performance, Electrochimica Acta. 370 (2021) 137755. https://doi.org/10.1016/j.electacta.2021.137755.

[48] N. Aristov, A. Habekost, Cyclic Voltammetry - A Versatile Electrochemical Method Investigating Electron Transfer Processes, World Journal of Chemical Education. (2015). https://doi.org/10.12691/wjce-3-5-2.

[49] J.I. Gowda, S.T. Nandibewoor, Electrochemical behavior of paclitaxel and its determination at glassy carbon electrode, Asian Journal of Pharmaceutical Sciences. (2014). https://doi.org/10.1016/j.ajps.2013.11.007.

[50] R.S. Nicholson, Irving. Shain, Theory of Stationary Electrode Polarography. Single Scan and Cyclic Methods Applied to Reversible, Irreversible, and Kinetic Systems., Analytical Chemistry. (1964). https://doi.org/10.1021/ac60210a007.

[51] T. Ohsaka, K. Hirabayashi, N. Oyama, Electrochemical Study on the Initial Stages of the Electropolymerization of 1-Pyrenamine in Acetonitrile, Bulletin of the Chemical Society of Japan. (1986). https://doi.org/10.1246/bcsj.59.3423.

[52] M. Pourbaix, Atlas of Electrochemical Equilibria in Aqueous Solutions, 2nd ed., National Association of Corrosion, 1974.

[53] A.J. Tkalych, K. Yu, E.A. Carter, Structural and Electronic Features of β-$Ni(OH)_2$ and β-NiOOH from First Principles, The Journal of Physical Chemistry. (2015). https://doi.org/10.1021/acs.jpcc.5b08481.

[54] X. Xiong, D. Ding, D. Chen, G. Waller, Y. Bu, Z. Wang, M. Liu, Three-dimensional ultrathin $Ni(OH)_2$ nanosheets grown on nickel foam for high-performance supercapacitors, Nano Energy. (2015). https://doi.org/10.1016/j.nanoen.2014.10.029.

[55] L. Li, J. Xu, J. Lei, J. Zhang, F. McLarnon, Z. Wei, N. Li, F. Pan, A one-step, cost-effective green

method to in situ fabricate $Ni(OH)_2$ hexagonal platelets on Ni foam as binder-free supercapacitor electrode materials, Journal of Materials Chemistry A. (2015). https://doi.org/10.1039/C4TA05156D.

[56] A.J. Bard, R. Parsons, J. Jordan, Standard Potentials in Aqueous Solution, 1st ed., Routledge, 2017. https://doi.org/10.1201/9780203738764.

[57] E.J.F. Dickinson, A.J. Wain, The Butler-Volmer equation in electrochemical theory: Origins, value, and practical application, Journal of Electroanalytical Chemistry. (2020). https://doi.org/10.1016/j.jelechem.2020.114145.

[58] J.S. Spendelow, A. Wieckowski, Electrocatalysis of oxygen reduction and small alcohol oxidation in alkaline media, Physical Chemistry Chemical Physics. (2007). https://doi.org/10.1039/b703315j.

[59] E. Hawlicka, R. Grabowski, Solvation and association of urea in aqueous solutions and mixtures of water with 1-propanol, Berichte Der Bunsengesellschaft Für Physikalische Chemie. (1994). https://doi.org/10.1002/bbpc.19940980610.

[60] L.G. Longsworth, Temperature Dependence of Diffusion in Aqueous Solutions, The Journal of Physical Chemistry. (1954). https://doi.org/10.1021/j150519a017.

[61] F. Wu, Z. Zhang, F. Zhang, D. Duan, Y. Li, G. Wei, S. Liu, Q. Yuan, E. Wang, X. Hao, New Insights into the Electrocatalytic Mechanism of Methanol Oxidation on Amorphous Ni-B-Co Nanoparticles in Alkaline Media, Catalysts. (2019). https://doi.org/10.3390/catal9090749.

[62] J.J. Medvedev, Y. Tobolovskaya, X.V. Medvedeva, S.W. Tatarchuk, F. Li, A. Klinkova, Pathways of ammonia electrooxidation on nickel hydroxide anodes and an alternative route towards recycled fertilizers, Green Chemistry. (2022). https://doi.org/10.1039/D1GC04140A.

[63] J. Brauns, J. Schönebeck, M.R. Kraglund, D. Aili, J. Hnát, J. Žitka, W. Mues, J.O. Jensen, K. Bouzek, T. Turek, Evaluation of Diaphragms and Membranes as Separators for Alkaline Water Electrolysis, Journal of The Electrochemical Society. (2021). https://doi.org/10.1149/1945-7111/abda57.

[64] Z. Liu, S.D. Sajjad, Y. Gao, H. Yang, J.J. Kaczur, R.I. Masel, The effect of membrane on an alkaline water electrolyzer, International Journal of Hydrogen Energy. (2017). https://doi.org/10.1016/j.ijhydene.2017.10.050.

[65] M. Duca, V. Kavvadia, P. Rodriguez, S.C.S. Lai, T. Hoogenboom, M.T.M. Koper, New insights into the mechanism of nitrite reduction on a platinum electrode, Journal of Electroanalytical Chemistry. (2010). https://doi.org/10.1016/j.jelechem.2010.01.019.

[66] K.I. Kuznetsov, S.V. Skorodumov, P.P. Granchenko, Measurements of the Dynamic Viscosity and Density of KOH Solutions at Atmospheric Pressure, High Temp. (2020). https://doi.org/10.1134/S0018151X20060127.

[67] G. Akerlof, P. Bender, The density of aqueous solutions of potassium hydroxide, Journal of the American Chemical Society. (1941). https://doi.org/10.1021/ja01849a054.

Appendices

Appendix A: Chemical and physicochemical data

All the information concerning chemicals and solutions used in this work is summarized in Table A.1.

Table A.1 Indexation of all chemicals and solutions used in this work

CAS n°	Name	Formula	Molecular weight ($g.mol^{-1}$)	Purity	Supplier	Batch n°
1310-73-2	Sodium hydroxide	NaOH	40.00	97%	Fisher Scientific	2181225
57-13-6	Urea	CON_2H_4	60.05	>99.5%	Sigma-Aldrich	SLCB9837
1310-58-3	Potassium hydroxide	KOH	56.11	85%	Alfa Aesar	10225535
7647-01-0	Hydrochloric acid	HCl	36.46	*wt*.37%	Fisher Scientific	2171489
75-75-2	Methanesulfonic acid	CH_4O_3S	96.10	99%	Acros Organics	A0419723
7632-00-0	Nitrite in aqueous solution	$Na^+ NO_2^-$	69.00	996 ± 8 $\mu g.mL^{-1}$	SCP Science	S2009A5024
12125-02-9	Ammonium in aqueous solution	$NH_4^+ Cl^-$	53.49	1006 ± 7 $\mu g.mL^{-1}$	SCP Science	S200407013
590-28-3	Potassium cyanate	KOCN	81.12	97%	Alfa Aesar	M08F008

The viscosities and densities of the solutions used in the electrochemical setups (containing urea and KOH) were measured.

The dynamic viscosities of solutions were measured at different temperatures (applied by Peltier effect) using a rheometer Physica MCR301 *Anton Paar®*, equipped with double-gap Couette system (standard measuring system DG26.7/T200/AL). To carry out these measurements, about 5 mL of each solution was used and the shear rates varied between 20 and 100 s^{-1}. Fig. A.1 shows the influence of the KOH concentration on the dynamic viscosity of the solutions prepared in this work. The viscosity of a water solution was added as a reference. A classical viscosity decay profile was observed with increasing temperature. As an example, the viscosity of a 1 M KOH solution decreased by 40% when varying the temperature from 288 to 313 K. Increasing the KOH concentration led to an increase in viscosity. For example, at 293 K, the increase in hydroxide concentration from 1 M to 5 M led to a 40% increased in viscosity. In addition, the present measurements were in agreement with the ones of Kuznetsov et al. [66].

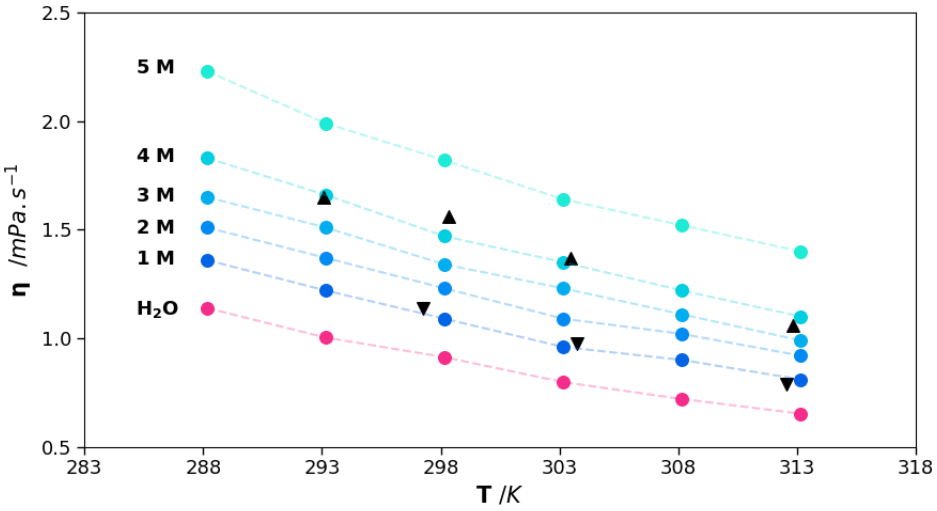

Fig. A.1 Effect of potassium hydroxide concentration on the dynamic viscosity of aqueous solutions. The black triangles up and down present data from the work of Kuznetsov et al. [66]

As shown in Fig. A.2, it was also verified that adding urea at a concentration of 0.33 mol.L^{-1} did not influence the viscosity of an alkaline solution.

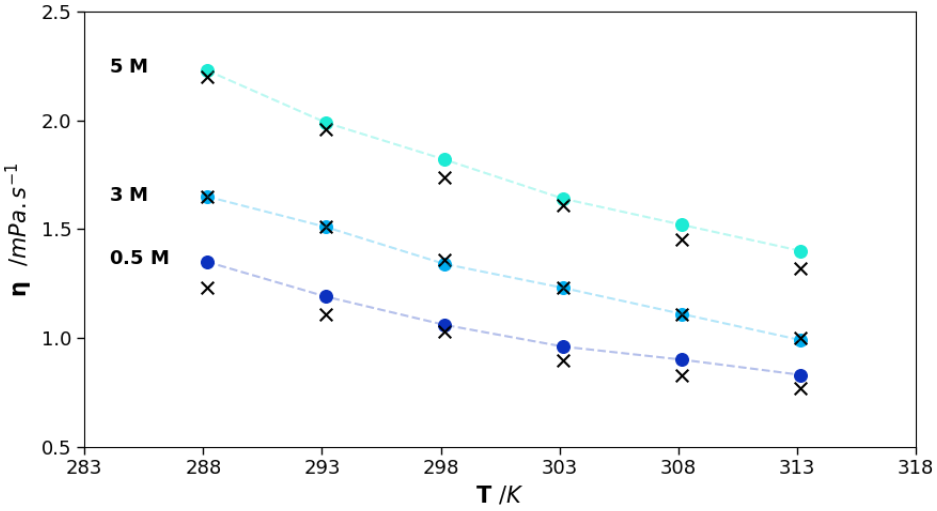

Fig. A.2 Effect of the presence of 0.33 mol.L^{-1} urea on the viscosity of alkaline solutions with different concentrations of potassium hydroxide. The crosses correspond to the viscosities of the alkaline solutions when adding urea at 0.33 mol.L^{-1}.

Density measurements were performed with a Densito 30 PX densitometer (*Mettler Toledo*®), with a thermoregulation at 293 K. Fig. A.3 shows the variation of the aqueous solution density as a function of KOH concentration in the aqueous solution. The values were in agreement with the ones of from Akerlof et

al. [67]. When comparing KOH solutions with and without urea at 0.33 mol.L^{-1}; no difference could be highlighted.

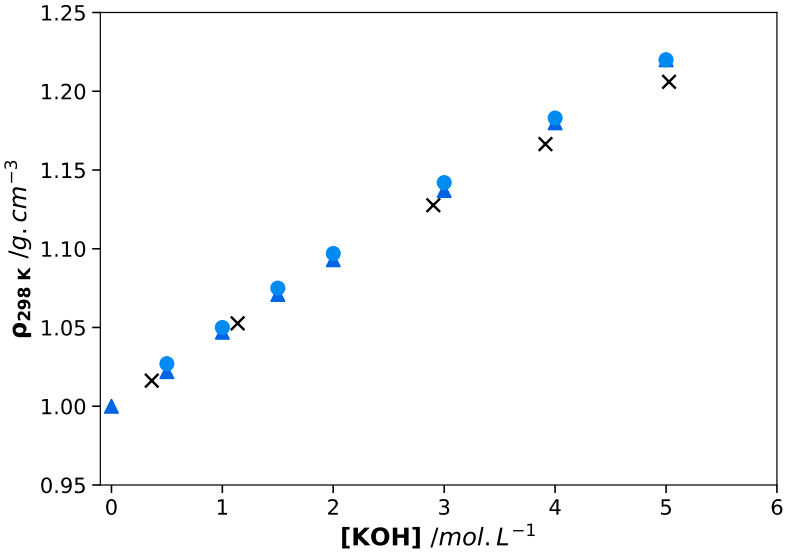

Fig. A.3 Effects of KOH concentration (triangle) and urea presence (dot) on the aqueous solution density at 298 K. The values extracted from Akerlof et al. [67] are illustrated with black cross.

Appendix B: Pictures of the different experimental setups

Fig. B.1 presents pictures of the three experimental set-ups used for i-E plot and electrolysis of urea alkaline solution, already illustrated schematically in the same order in Fig. 1.

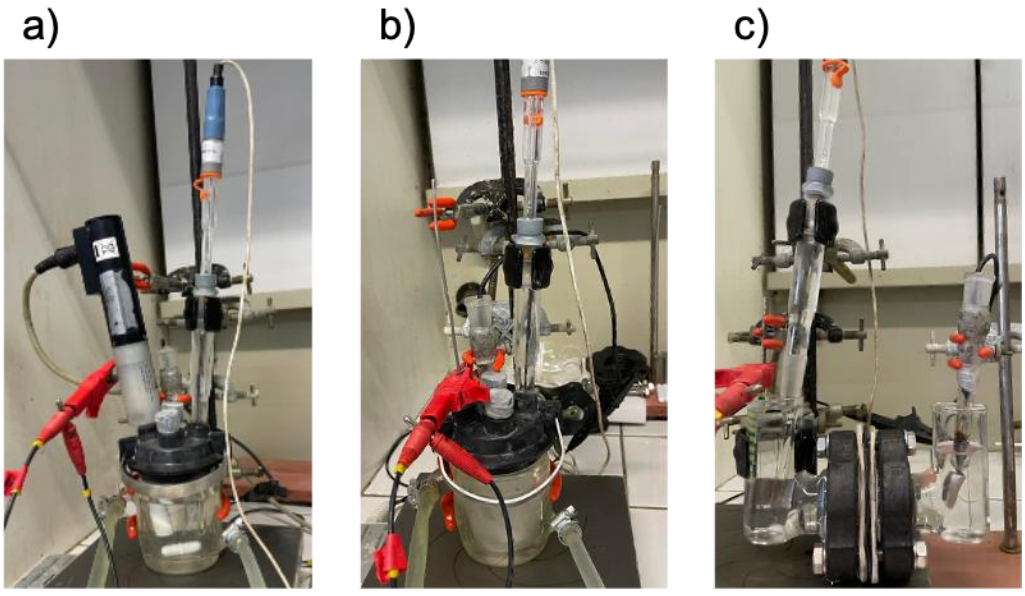

Fig. B.1 Experimental set-ups for i-E plot and electrolysis of urea alkaline solution.

Appendix C: Analysis by ionic chromatography analysis

Ionic chromatography analysis allowed identifying and quantifying the electrogenerated ionic byproducts present during the electrolysis experiments. A graph showing the applied concentration gradient of the eluent against time is shown in Fig.C.1.

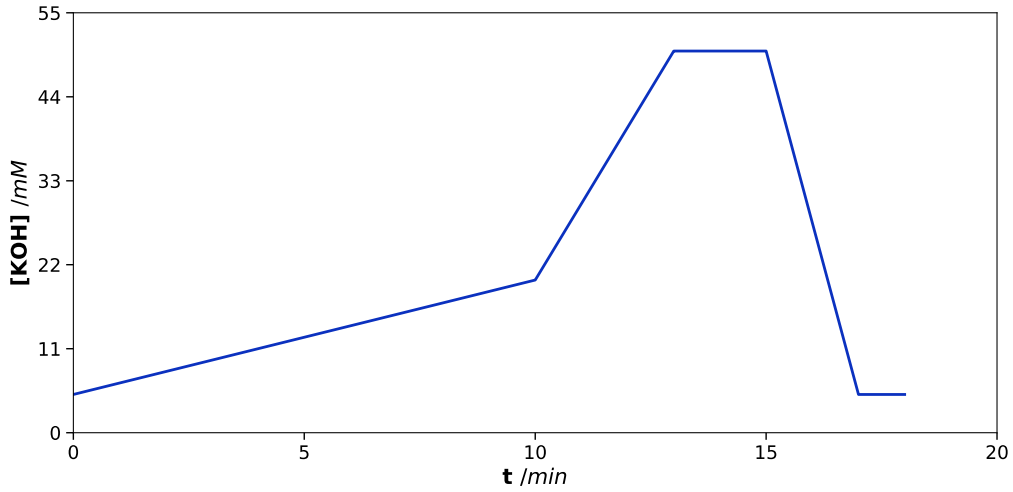

Fig. C.1 Temporal profile of the eluent (KOH) concentration during the analysis of anions by ionic chromatography

Typical chromatograms and calibration curves are shown in Fig. C.2.

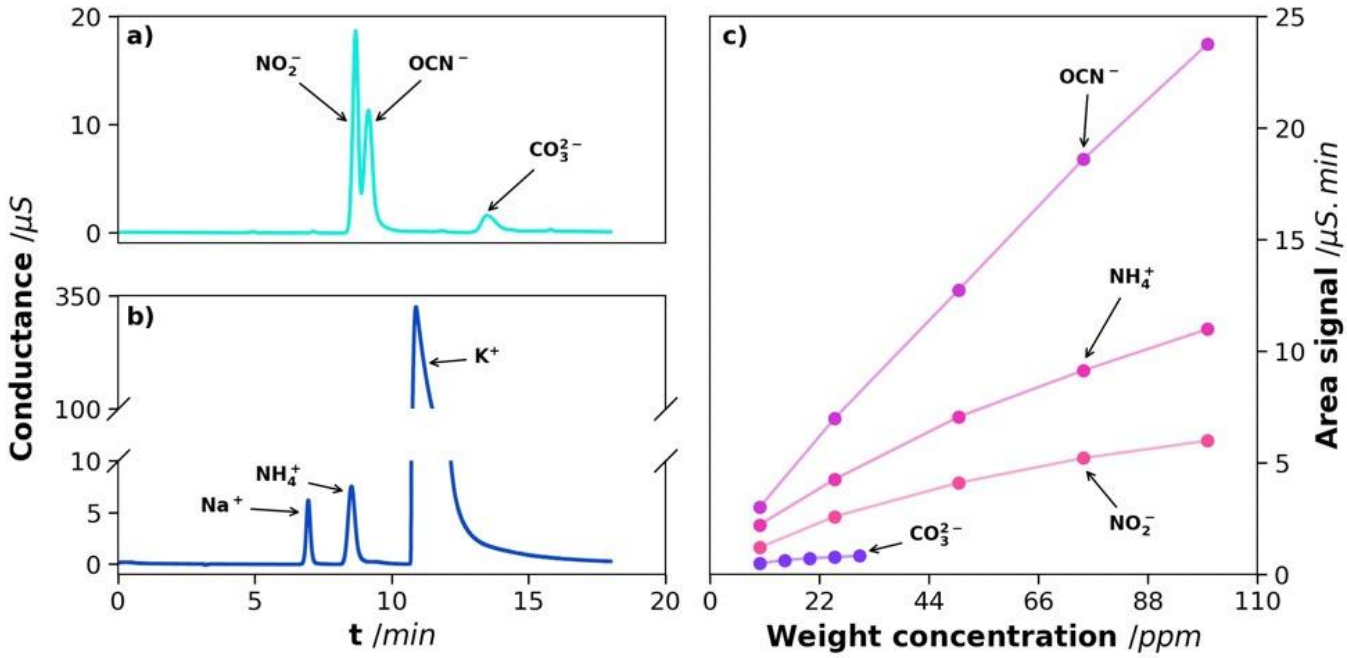

Fig. C.2 Typical anionic (a) and cationic (b) chromatographs obtained during urea electrolysis experiment, and calibration curves (c) for the major byproducts formed during urea electrolysis.

Appendix D: Non Purgeable Organic Carbon (NPOC) analysis

The carbon compounds identified during electrolysis were urea and cyanate as organic carbon, and carbonate as inorganic carbon. Among organic carbon, two subcategories could be identified, namely purgeable organic carbon (POC) and NPOC. When measuring NPOC, an excess of hydrochloric acid was poured in to acidify the sample so that inorganic matter and weak acids (cyanate in our case) were removed as CO_2 gas or volatile acid (cyanic acid in the present case). It was therefore necessary to verify that the NPOC measurement allowing direct access to the urea concentration was not deviated by the presence of cyanate in the sample. To do this, various alkaline standards with urea and cyanate concentrations were prepared and then analyzed to determine the corresponding NPOC values. The results, shown in Table D.1, confirmed the direct relationship between NPOC measurements and urea concentrations.

Table D.1 Evidence of the direct relationship between NPOC measurements and urea concentrations

Sample	**$[CO(NH_2)_2]$ (mol.L^{-1})**	**$[CO(NH_2)_2]$ (*eq C* g.L^{-1})**	**$[OCN^-]$ (mol.L^{-1})**	**$[OCN^-]$ (*eq C* g.L^{-1})**	**$[NPOC]_{result}$ (*eq C* g.L^{-1})**
1	0.3	3.6	0	0	3.6 ± 0.2

2	0.2	2.4	0.1	1.2	2.4 ± 0.2
3	0.1	1.2	0.2	2.4	1.2 ± 0.2
4	0	0	0.3	3.6	0.12

Appendix E: Evolution of the anodic peak potential against the logarithm of the potential scan rate

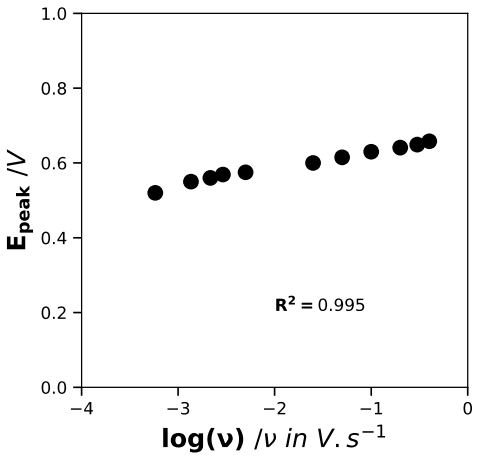

Fig. E.1 Evolution of the anodic peak potential against the logarithm of the potential scan rate

Appendix F: Evolution of the current magnitude of the anodic peak against the potential scan rate

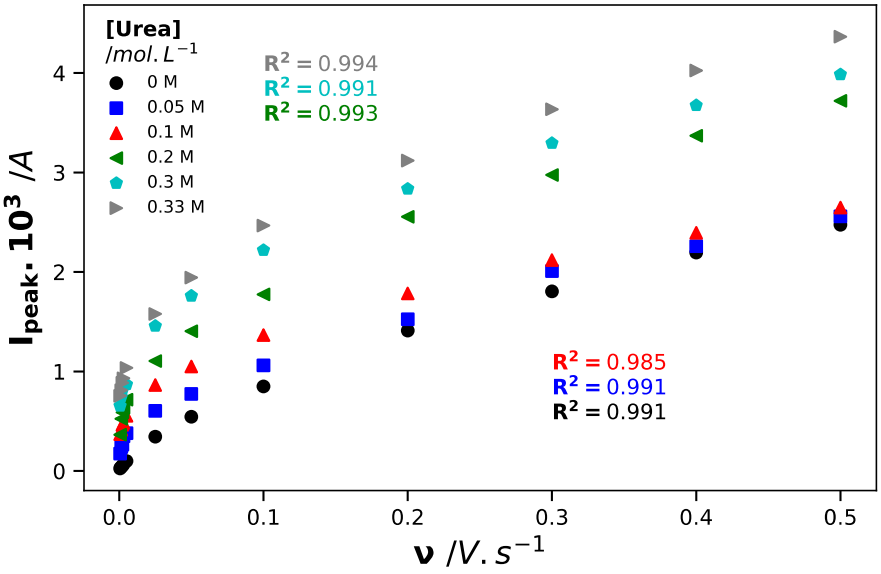

Fig. F. 1 Evolution of the current magnitude of anodic peak against the potential scan rate

Appendix G: Pourbaix diagram of nickel

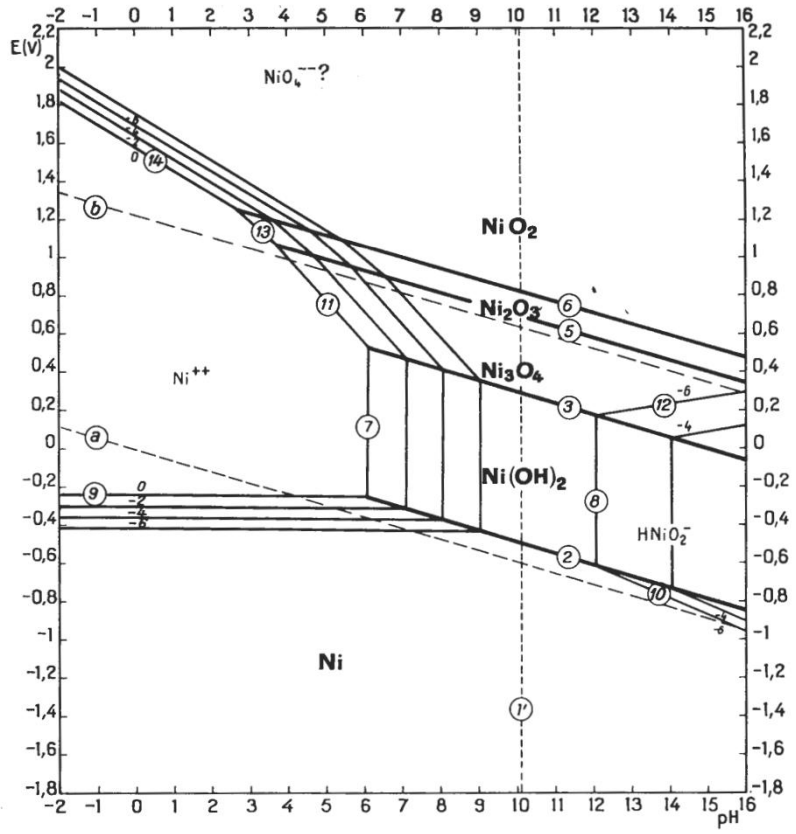

Fig. G.1 Potential-pH equilibrium diagram for the system nickel-water at 298 K (Extracted from [52])